

Long-lived melting of ancient lower crust of the North China Craton in response to paleo-Pacific plate subduction, recorded by adakitic rhyolite

Chao Wang ^{a,b,*}, Shuguang Song ^{a,**}, Yaoling Niu ^{b,c}, Mark B. Allen ^b, Li Su ^d, Chunjing Wei ^a, Guibin Zhang ^a, Bin Fu ^e

^a MOE Key Laboratory of Orogenic Belts and Crustal Evolution, School of Earth and Space Sciences, Peking University, Beijing 100871, China

^b Department of Earth Sciences, Durham University, Durham DH1 3LE, UK

^c Institute of Oceanology, Chinese Academy of Science, Qingdao 266071, China

^d School of Scientific Research, State Key Laboratory of Geological Processes and Mineral Resources, Chinese University of Geosciences, Beijing 100083, China

^e Research School of Earth Sciences, The Australian National University, Canberra, ACT 2601, Australia

ARTICLE INFO

Article history:

Received 24 June 2017

Accepted 29 September 2017

Available online 7 October 2017

Keywords:

Adakitic rhyolite

Long-lived lower crustal melting

Cratonic destruction

Paleo-Pacific plate subduction

North China Craton

ABSTRACT

Magmatism in eastern China in response to paleo-Pacific plate subduction during the Mesozoic was complex, and it is unclear how and when exactly the magmas formed via thinning and partial destruction of the continental lithosphere. To better understand this magmatism, we report the results of a geochronological and geochemical study of Early Cretaceous adakitic rhyolite (erupted at 125.4 ± 2.2 Ma) in the Xintaimen area within the eastern North China Craton (NCC). *In situ* zircon U-Pb dating shows that this adakitic rhyolite records a long (~70 Myrs) and complicated period of magmatism with concordant $^{206}\text{Pb}/^{238}\text{U}$ ages from 193 Ma to 117 Ma. The enriched bulk rock Sr-Nd isotopic compositions of the Xintaimen adakitic rhyolite, as well as the enriched zircon Hf and O isotopic compositions, indicate that the magmas parental to the adakitic rhyolite were derived from partial melting of the Paleoproterozoic mafic lower crust, heated by mafic melts derived from the mantle during the paleo-Pacific plate subduction. A minor older basement component is indicated by the presence of captured Neoarchean to Early Paleoproterozoic zircons. The Mesozoic zircons have restricted Hf and O isotopic compositions irrespective of their ages, suggesting that they formed from similar sources at similar melting conditions. The Xintaimen adakitic rhyolite offers an independent line of evidence that the ancient lower crust of eastern China underwent a long period (~70 Myrs) of destruction, melting or remelting, from ~193 to ~120 Ma, related to the subduction of the paleo-Pacific plate beneath eastern China.

© 2017 Elsevier B.V. All rights reserved.

1. Introduction

The North China Craton (NCC) experienced significant lithospheric destruction and thinning since the Mesozoic, and has consequently been a research focus over the past decades (e.g., Gao et al., 2004; Niu, 2005, 2014; Xu, 2001; Yang et al., 2010). The sharp compositional contrast between mantle xenoliths recovered from Paleozoic kimberlites and Cenozoic basalts suggests that a thick (>180 km), cold and refractory lithospheric keel in the Paleozoic was replaced by a thin (<100 km), hot and fertile lithosphere (e.g., Menzies et al., 2007; Zheng et al., 2006). It is generally acknowledged that the destruction or thinning of the NCC lithosphere began in the Triassic (~230–220 Ma) and took place diachronously for >100 Myrs (Wang et al., 2015; Wu et al., 2005b; Xu et al., 2006, 2009; Yang et al., 2008, 2010; S.-H. Zhang et al., 2014).

This destruction was the result of the interactions between the NCC and adjacent blocks, including the paleo-Asian plate, the Yangtze Craton, the Siberian plate and the paleo-Pacific plate (e.g., Gao et al., 2004; Liu et al., 2008; Menzies et al., 2007; Niu, 2005, 2014; Zhang, 2012). Various mechanisms of cratonic destruction have been proposed in the literature (e.g., Gao et al., 2004; Menzies et al., 2007; Niu, 2005, 2014; Wang et al., 2015; Wu et al., 2005a, 2005b).

Mesozoic igneous rocks are widespread in eastern China with an overall NE-SW trend in outcrop, from South China, through the NCC, to NE China. Most of them were emplaced and/or erupted from the Jurassic to the Early Cretaceous, with a small volume being of Triassic age. These Mesozoic igneous rocks can provide us the information on how and when exactly the lithosphere beneath eastern China was thinned (Niu et al., 2015; Wang et al., 2013; Wu et al., 2005a, 2011; S.-H. Zhang et al., 2014; Zhou et al., 2006).

It is generally accepted that paleo-Pacific plate subduction played an important role in the Mesozoic magmatism in eastern China (Ma et al., 2016; Niu, 2005; Niu et al., 2015; Wang et al., 2013; Wu et al., 2005b, 2011; S.-H. Zhang et al., 2014; Zhou et al., 2006). However, the timing of onset of paleo-Pacific plate subduction beneath eastern

* Correspondence to: C. Wang, MOE Key Laboratory of Orogenic Belts and Crustal Evolution, School of Earth and Space Sciences, Peking University, Beijing 100871, China.

** Corresponding author.

E-mail addresses: daniel.wangchao@gmail.com, chaowang@pku.edu.cn (C. Wang), sgsong@pku.edu.cn (S. Song).

China remains controversial, with different suggestions including the Early Permian (e.g., X.-H. Li et al., 2012; Z.-X. Li et al., 2012; Li and Li, 2007; Sun et al., 2015), the Early Triassic (e.g., Liu et al., 2017) and the Late Triassic to the Early Jurassic (e.g., Guo et al., 2015; Zhou et al., 2014). Niu et al. (2015) proposed that paleo-Pacific plate subduction ceased at 100–90 Ma as the result of trench-jam in the southeast continental China. Tang et al. (2016), however, suggested that the paleo-Pacific plate subduction could have continued until 56 Ma in the north, inferred from the intrusion ages of younger granitoids in the Korean Peninsula (>71 Ma), Southwest Japan (>71 Ma) and Far East Russia (>56 Ma) (Niu and Tang, 2016; Tang et al., 2016). The timing of the onset and termination of the paleo-Pacific plate subduction, and its relationship to the destruction of NCC, require further study.

In this contribution, we present a combined study of zircon U-Pb dating, bulk rock elemental and Sr-Nd isotope geochemistry and *in situ* zircon Hf-O isotope analyses for adakitic rhyolite in the Xintaimen area, eastern China. We show that the Xintaimen adakitic rhyolite was formed by melting of the Paleoproterozoic mafic lower crust, triggered by heating from the underplating mantle-derived mafic melts in the Mesozoic. We demonstrated that this melting process lasted for ~70 Myrs from the onset (~193 Ma) to the late stage (~120 Ma) of the paleo-Pacific plate subduction beneath the eastern continental China. Thus, the Xintaimen adakitic rhyolite records a long-lived destruction/melting process of the ancient lower crust of the eastern continental China in response to the paleo-Pacific plate subduction.

2. Geological background and petrology

The NCC is the largest and oldest craton in China and it preserves remnants of ancient (≥ 3.8 Ga) crustal records (Liu et al., 1992; Song et al., 1996). The NCC was formed by collision of micro-continents at the end of the Archean (e.g. Wang et al., 2016), and finally by amalgamation of the Eastern and Western blocks along the Trans-North China Orogen in the Late Paleoproterozoic (Zhao et al., 2005). From the Late

Paleoproterozoic to the end of the Paleozoic, most parts of the NCC remained geologically inactive except for some episodic and sporadically distributed mantle plume-related magmatism during the Proterozoic (e.g., Peng et al., 2012; Zhang et al., 2017). However, since the Mesozoic, volumetrically significant magmatism occurred throughout eastern China (e.g., Niu et al., 2015; Wu et al., 2005a, 2005b; Yang and Wu, 2009; S.-H. Zhang et al., 2014). Detailed geochronological studies show that most of these Mesozoic magmas formed during the Late Jurassic (180–153 Ma) and the Early Cretaceous (135–110 Ma), with minor magmatism being Triassic (231–210 Ma) (Wang et al., 2015; Wu et al., 2005a, 2005b; Yang and Wu, 2009).

The study area lies west of the Tan-Lu fault, near Xingcheng, in western Liaoning, in the eastern segment of the northern margin of the NCC (Fig. 1a). Archean basement rocks in this area mainly occur along the west coast of the Bohai Sea and consist of Neoproterozoic tonalite-trondhjemite-granodiorite (TTG) and potassio granitoids with coeval mafic magmatic enclaves (Fig. 1a; Wang et al., 2016). Mesozoic volcano-sedimentary sequences belong to four major pulses of volcanism, represented by the Xinglonggou Formation (177 Ma; basalt), the Lanqi Formation (166–153 Ma; basalt, basaltic andesite, andesite and rhyolite), the Yixian Formation (126–120 Ma; basalt, basaltic andesite, andesite and rhyolite) and the Zhanglaogongtun Formation (~106 Ma; andesite and dacite) (Fig. 1; Gao et al., 2004, 2008; Yang and Li, 2008). Mesozoic intermediate-felsic plutons also occur in this region (Fig. 1; Wu et al., 2006; Zhang et al., 2010; X. Zhang et al., 2014).

The studied samples were collected from a volcanic plug showing columnar jointing (Fig. 2a and b) surrounded by explosive breccia within the Cretaceous Yixian Formation (Yang and Li, 2008) near Xintaimen town (Fig. 1). They display porphyritic textures with plagioclase, amphibole and minor clinopyroxene as phenocrysts in the groundmass (Fig. 2c). Plagioclase phenocrysts are mostly subhedral to euhedral without later alteration. Amphibole phenocrysts are euhedral with dark rims. Clinopyroxene phenocrysts are rare, but present in some

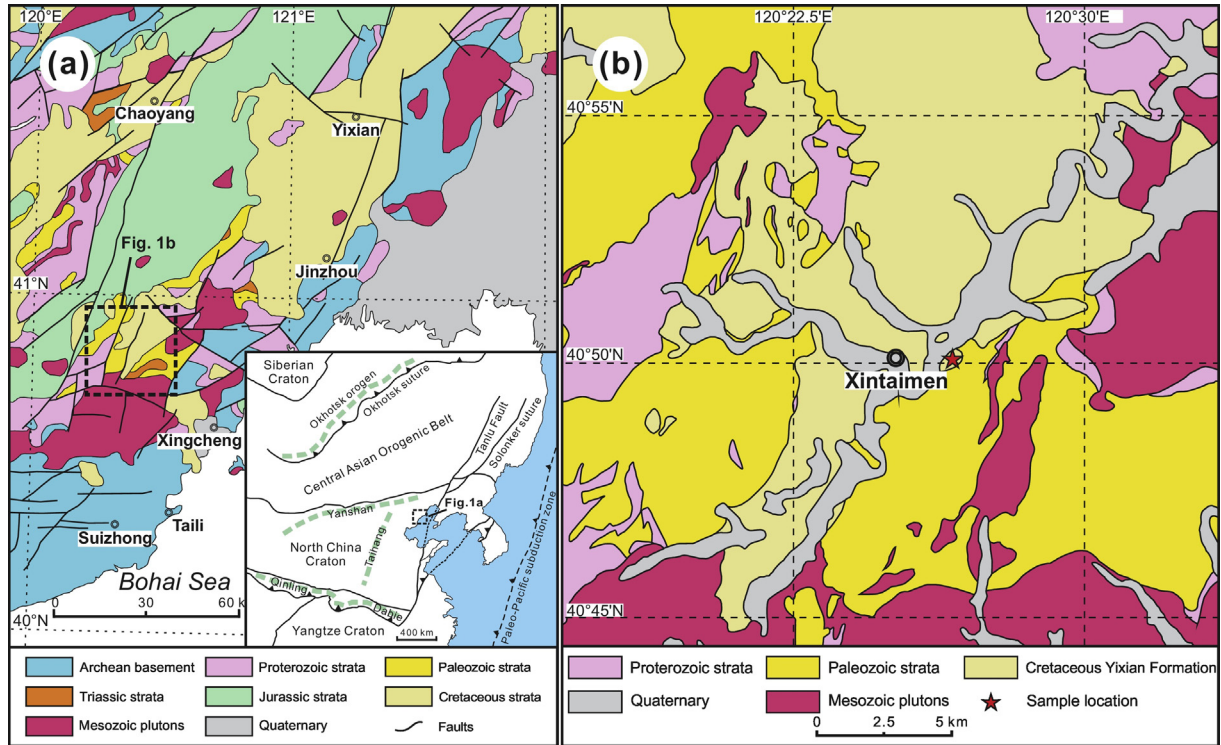


Fig. 1. (a) Simplified geological map of western Liaoning in eastern NCC; inset is the geodynamic map showing interactions between the NCC and surrounding blocks. (b) Simplified geological map of the Xintaimen area in the Xingcheng region.

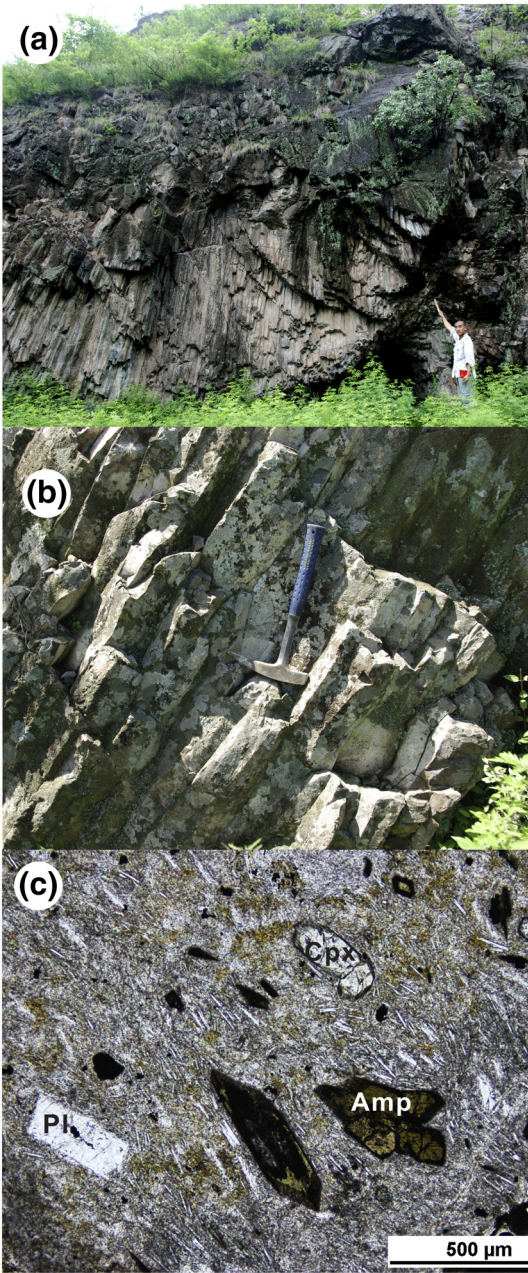


Fig. 2. (a) and (b) Field photo of the Xintaimen rhyolite. Note that they show typical columnar jointing. (c) Photomicrograph (plane-polarized light) showing the petrographic features of the Xintaimen rhyolite. Pl, plagioclase; Amp, amphibole; Cpx, clinopyroxene.

samples and are subhedral to euhedral. Their groundmass consists of fine-grained quartz, plagioclase, K-feldspar and opaque oxides.

3. Analytical methods

Geochemical data presented in this study include bulk rock major and trace element compositions, Sr-Nd isotopes and *in situ* zircon U-Pb, Hf and O isotopes; all the data are given in Tables 1–5.

Zircon grains were extracted from crushed samples by standard heavy-liquid and magnetic techniques, and purified by hand-picking under a binocular microscope. Cathodoluminescence (CL) images were acquired using a cathodoluminescent spectrometer (Garton Mono CL3+) equipped on a Quanta 200F ESEM at Peking University. Measurements of U, Th and Pb in zircons were carried out on an Agilent-7500a quadrupole inductively coupled plasma mass spectrometer coupled

with a New Wave UP-193 solid-state laser-ablation system (LA-ICP-MS) in the Geological Lab Center, China University of Geosciences, Beijing (CUGB). A detailed account of operating conditions, standards, and data reduction and plot processes are given in Song et al. (2010a). Sixty-nine zircon grains were also analyzed by SHRIMP (Sensitive High Resolution Ion Micro-Probe) II as a double-check in the Research School of Earth Sciences, The Australian National University, Canberra, Australia (see details in the Appendix).

Bulk rock major and trace element analysis was done at CUGB. Major elements were analyzed on a Leeman Prodigy inductively coupled plasma-optical emission spectroscopy (ICP-OES) system with high dispersion Echelle optics. Trace elements were analyzed using an Agilent-7500a quadrupole inductively coupled plasma mass spectrometry (ICP-MS). Detailed operating conditions, sample digestion procedures, standard materials and analytical precision and accuracy are described in Song et al. (2010b) and Wang et al. (2016).

Separation and purification of Sr and Nd were carried out using conventional ion exchange procedures in the ultraclean laboratory of MOE Key Laboratory of Orogenic Belts and Crustal Evolution, Peking University. Sr and Nd isotopic ratios were measured using a Thermo-Finnigan Triton thermal ionization mass spectrometer at the Isotope Laboratory of Tianjin Institute of Geology and Mineral Resources. Sample digestion, standards and mass fraction correction procedures are described in Wang et al. (2016).

In situ zircon Lu-Hf isotope analysis of the dated sample 12XTM01 was carried out using a Neptune multi-collector ICP-MS attached with a New Wave UP-213 laser-ablation system (LA-MC-ICP-MS) at MLR Key Laboratory of Metallogeny and Mineral Assessment, Institute of Mineral Resources, Chinese Academy of Geological Sciences, Beijing. Detailed operating conditions, standards and correction procedures for isobaric interferences are described in Wang et al. (2016).

In situ zircon oxygen isotopes for the dated sample 12XTM01 were analyzed using SHRIMP II in the Research School of Earth Sciences, The Australian National University, Canberra, Australia. The instrumental conditions and measurement procedures were similar to those reported by Ireland and Williams (2003) and Ickert et al. (2008). The instrumental mass fractionation factor was corrected using the FC-1 zircon standard with $\delta^{18}\text{O}_{\text{VSMOW}} = 5.61 \pm 0.14\text{\textperthousand}$ (2σ SD, $n = 6$; John W. Valley, unpublished data; c.f. Fu et al., 2015). Corrected $^{18}\text{O}/^{16}\text{O}$ ratios are reported in ^{18}O notation, in permil variations relative to Vienna standard mean ocean water (VSMOW, $^{18}\text{O}/^{16}\text{O} = 0.0020052$). Spot-to-spot uncertainty (or external error) was typically better than $\pm 0.6\text{\textperthousand}$ (2σ) for ^{18}O . During the analysis, the average ^{18}O of the secondary standard zircon (TEMORA-2) was $8.05 \pm 0.15\text{\textperthousand}$ (2σ SD, $n = 15$).

4. Results

4.1. *In situ* zircon U-Pb zircon ages

Zircon grains from Xintaimen rhyolite sample 12XTM01 are all euhedral-prismatic and in CL images show typical oscillatory growth zoning of magmatic origin without any relict cores (Fig. 3a). They have a wide range in Th/U ratios of 0.29–3.08 (Table 1). One hundred and sixty zircons were analyzed giving a wide range of ages (Table 1). In the conventional U-Pb concordia diagram (Fig. 3b), most of the zircons plot on the concordia. As shown in the zircon age histogram (Fig. 3c), these zircons cluster in three distinct groups: (1) 37 grains yield Neoarchean to Early Paleoproterozoic $^{207}\text{Pb}/^{206}\text{Pb}$ ages from 2603 ± 20 to 2463 ± 15 Ma, although some of the grains are discordant possibly due to lead loss; (2) 116 grains give concordant Jurassic $^{206}\text{Pb}/^{238}\text{U}$ ages from 193 ± 4 to 146 ± 5 Ma; and (3) 14 grains show a narrow range in the Early Cretaceous with $^{206}\text{Pb}/^{238}\text{U}$ ages from 131 ± 3 Ma to 117 ± 3 Ma; these concordant analyses give a weighted mean $^{206}\text{Pb}/^{238}\text{U}$ age of 125.4 ± 2.2 Ma (2σ , MSWD = 1.8) (Table 1). The sixty-nine zircons also analyzed

Table 1*In situ* LA-ICP-MS zircon U-Pb data for the Xintaimen rhyolite.

Spot	Concentrations (ppm)			Th/U			Isotopic ratios			Isotopic ages (Ma)								
	Pb	U	Th		$^{207}\text{Pb}/^{206}\text{Pb}^a$	$\pm 1\sigma$	$^{207}\text{Pb}/^{235}\text{U}$	$\pm 1\sigma$	$^{206}\text{Pb}/^{238}\text{U}$	$\pm 1\sigma$		$^{207}\text{Pb}/^{206}\text{Pb}$	$\pm 1\sigma$	$^{207}\text{Pb}/^{235}\text{U}$	$\pm 1\sigma$	$^{206}\text{Pb}/^{238}\text{U}$	$\pm 1\sigma$	
<i>12XTM01</i>																		
1.1	2	67	64	0.95	0.04919		0.00329	0.16788	0.01099	0.02475	0.00048	157		112	158	10	158	3
1.2	5	134	108	0.81	0.04950		0.00325	0.18684	0.01215	0.02737	0.00043	172		118	174	10	174	3
1.3	9	297	212	0.72	0.05204		0.00386	0.17186	0.01243	0.02395	0.00039	287		171	161	11	153	2
1.4	71	111	79	0.71	0.17075		0.00364	11.53391	0.24667	0.48975	0.00648	2565		19	2567	20	2570	28
1.5	5	140	127	0.91	0.04958		0.00296	0.18988	0.01108	0.02777	0.00050	175		100	177	9	177	3
1.6	0	10	9	0.87	0.04890		0.00573	0.15441	0.01228	0.02290	0.00072	143		1018	146	10	146	5
1.7	5	167	77	0.46	0.04924		0.00403	0.16329	0.01327	0.02404	0.00040	159		152	154	12	153	3
1.8	83	139	42	0.30	0.17188		0.00375	11.61875	0.25405	0.49012	0.00660	2576		19	2574	20	2571	29
1.9	2	63	88	1.39	0.04944		0.00847	0.17772	0.03007	0.02606	0.00079	169		286	166	26	166	5
1.10	7	202	192	0.95	0.04938		0.00348	0.17397	0.01213	0.02554	0.00042	166		127	163	10	163	3
1.11	1	17	9	0.56	0.04959		0.01830	0.18405	0.06756	0.02691	0.00110	176		566	172	58	171	7
1.12	9	211	385	1.83	0.04934		0.00207	0.18004	0.00737	0.02646	0.00042	164		66	168	6	168	3
1.13	7	197	147	0.75	0.04960		0.00219	0.18855	0.00813	0.02756	0.00045	176		70	175	7	175	3
1.14	1	35	47	1.33	0.04986		0.00917	0.20703	0.03758	0.03011	0.00098	188		308	191	32	191	6
1.15	84	137	60	0.43	0.16911		0.00370	11.30437	0.24764	0.48468	0.00647	2549		20	2549	20	2548	28
1.16	3	101	79	0.79	0.04946		0.00378	0.17622	0.01327	0.02584	0.00049	170		134	165	11	164	3
1.17	9	228	234	1.02	0.04968		0.00237	0.19863	0.00929	0.02899	0.00047	180		79	184	8	184	3
1.18	92	134	104	0.77	0.17463		0.00392	11.98453	0.26849	0.49759	0.00676	2603		20	2603	21	2603	29
1.19	11	296	403	1.36	0.04944		0.00248	0.17211	0.00851	0.02524	0.00040	169		85	161	7	161	3
1.20	58	101	99	0.97	0.16959		0.00384	9.43902	0.21303	0.40355	0.00548	2554		20	2382	21	2185	25
1.21	7	215	99	0.46	0.04952		0.00231	0.18410	0.00839	0.02696	0.00045	173		75	172	7	171	3
1.22	11	306	306	1.00	0.04951		0.00267	0.18049	0.00959	0.02643	0.00042	172		93	168	8	168	3
1.23	11	236	464	1.96	0.04964		0.00296	0.19098	0.01121	0.02789	0.00047	178		103	177	10	177	3
1.24	4	134	81	0.61	0.04903		0.00482	0.15879	0.01536	0.02348	0.00051	149		176	150	13	150	3
1.25	2	39	43	1.11	0.04605		0.00991	0.16791	0.03575	0.02645	0.00084	–		–	158	31	168	5
1.26	7	212	180	0.85	0.04924		0.00343	0.16791	0.01157	0.02473	0.00041	159		124	158	10	157	3
1.27	16	394	466	1.18	0.04977		0.00249	0.19460	0.00966	0.02835	0.00042	184		88	181	8	180	3
1.28	13	357	391	1.10	0.04943		0.00245	0.17590	0.00861	0.02580	0.00039	168		85	165	7	164	2
1.29	12	252	549	2.18	0.04942		0.00273	0.18134	0.00984	0.02661	0.00045	168		93	169	8	169	3
1.30	7	165	214	1.30	0.04950		0.00531	0.18828	0.02003	0.02758	0.00055	172		202	175	17	175	3
2.1	1	33	54	1.65	0.04860		0.00798	0.13280	0.02177	0.01982	0.00056	129		279	127	20	127	4
2.2	11	306	317	1.04	0.04605		0.00270	0.17653	0.00965	0.02780	0.00058	–		–	165	8	177	4
2.3	12	333	247	0.74	0.04969		0.00130	0.19464	0.00603	0.02840	0.00058	181		37	181	5	181	4
2.4	7	219	173	0.79	0.04967		0.00187	0.19191	0.00788	0.02802	0.00059	180		57	178	7	178	4
2.5	125	247	74	0.30	0.16317		0.00522	9.75968	0.24094	0.43381	0.00882	2489		55	2412	23	2323	40
2.6	41	119	95	0.80	0.16221		0.00237	6.10116	0.13711	0.27275	0.00553	2479		17	1990	20	1555	28
2.7	0	12	13	1.09	0.04932		0.01761	0.16945	0.06023	0.02491	0.00111	163		538	159	52	159	7
2.8	5	163	115	0.70	0.04908		0.00263	0.15924	0.00887	0.02352	0.00051	152		88	150	8	150	3
2.9	349	536	631	1.18	0.16842		0.00237	11.05633	0.24559	0.47603	0.00962	2542		17	2528	21	2510	42
2.10	44	71	65	0.91	0.16762		0.00252	10.93134	0.24903	0.47289	0.00967	2534		17	2517	21	2496	42
2.11	5	150	157	1.05	0.04941		0.00193	0.17396	0.00734	0.02553	0.00055	167		59	163	6	163	3
2.12	6	159	194	1.22	0.04940		0.00247	0.17843	0.00935	0.02619	0.00057	167		81	167	8	167	4
2.13	6	177	168	0.95	0.04953		0.00177	0.18815	0.00736	0.02754	0.00059	173		52	175	6	175	4
2.14	69	137	58	0.42	0.16389		0.00564	9.38940	0.25578	0.41551	0.00872	2496		59	2377	25	2240	40
2.15	6	202	137	0.68	0.04940		0.00196	0.17257	0.00733	0.02533	0.00055	167		59	162	6	161	3
2.16	33	842	911	1.08	0.04997		0.00099	0.20909	0.00546	0.03034	0.00063	194		28	193	5	193	4
2.17	5	179	104	0.58	0.04932		0.00229	0.17340	0.00850	0.02549	0.00055	163		74	162	7	162	3
2.18	13	341	355	1.04	0.04987		0.00125	0.20450	0.00619	0.02973	0.00062	189		35	189	5	189	4
2.19	14	399	486	1.22	0.04942		0.00120	0.18060	0.00533	0.02650	0.00055	168		34	169	5	169	3
2.20	26	700	1013	1.45	0.04948		0.00103	0.18524	0.00498	0.02715	0.00056	171		29	173	4	173	4
2.21	138	257	110	0.43	0.16549		0.00250	10.34651	0.23841	0.45335	0.00931	2513		17	2466	21	2410	41
2.22	23	556	816	1.47	0.05287		0.00126	0.21922	0.00640	0.03006	0.00063	323		32	201	5	191	4
2.23	8	193	349	1.81	0.04605		0.00272	0.16353	0.00899	0.02576	0.00055	–		–	154	8	164	3
2.24	6	163	296	1.82	0.04919		0.00239	0.16831	0.00862	0.02481	0.00054	157		79	158	7	158	3
2.25	207	372	353	0.95	0.16856		0.00258	9.74733	0.22615	0.41930	0.00863	2543		17	2411	21	2257	39
2.26	12	309	343	1.11	0.04995		0.00135	0.20828	0.00665	0.03023	0.00064	193		38	192	6	192	4
2.27	7	224	154	0.69	0.04940		0.00182	0.17836	0.00719	0.02618	0.00057	167		54	167	6	167	4
2.28	14	437	446	1.02	0.04935		0.00125	0.17474	0.00534	0.02567	0.00054	164		35	164	5	163	3
2.29	18	491	788	1.61	0.04939		0.00114	0.17905	0.00513	0.02628	0.00055	166		32	167	4	167	3
2.30	7	201	256	1.28	0.04925		0.00											

Table 1 (continued)

Spot	Concentrations (ppm)			Th/U Isotopic ratios						Isotopic ages (Ma)						
	Pb	U	Th	$^{207}\text{Pb}/^{206}\text{Pb}^a$	$\pm 1\sigma$	$^{207}\text{Pb}/^{235}\text{U}$	$\pm 1\sigma$	$^{206}\text{Pb}/^{238}\text{U}$	$\pm 1\sigma$	$^{207}\text{Pb}/^{206}\text{Pb}$	$\pm 1\sigma$	$^{207}\text{Pb}/^{235}\text{U}$	$\pm 1\sigma$	$^{206}\text{Pb}/^{238}\text{U}$	$\pm 1\sigma$	
2.43	29	682	1600	2.35	0.04936	0.00110	0.17604	0.00498	0.02586	0.00055	165	31	165	4	165	3
2.44	17	460	722	1.57	0.05218	0.00580	0.18339	0.01988	0.02549	0.00063	293	255	171	17	162	4
2.45	4	115	101	0.88	0.04940	0.00366	0.17449	0.01319	0.02561	0.00060	167	127	163	11	163	4
2.46	14	430	499	1.16	0.05055	0.00179	0.17970	0.00703	0.02578	0.00057	220	51	168	6	164	4
2.47	2	48	54	1.13	0.04605	0.00439	0.16047	0.01481	0.02528	0.00061	–	–	151	13	161	4
2.48	7	199	213	1.07	0.04961	0.00171	0.19297	0.00740	0.02821	0.00063	177	49	179	6	179	4
2.49	8	227	233	1.02	0.04976	0.00189	0.19403	0.00807	0.02827	0.00063	184	56	180	7	180	4
2.50	12	320	556	1.74	0.05410	0.00192	0.20447	0.00804	0.02741	0.00061	375	50	189	7	174	4
2.51	1	31	29	0.93	0.04921	0.00839	0.17586	0.02992	0.02591	0.00076	158	290	164	26	165	5
2.52	9	285	293	1.03	0.04927	0.00181	0.16971	0.00685	0.02498	0.00056	161	54	159	6	159	4
2.53	4	71	179	2.52	0.06712	0.01313	0.24726	0.04774	0.02672	0.00085	842	439	224	39	170	5
2.54	9	215	182	0.84	0.05230	0.00595	0.19417	0.02152	0.02693	0.00068	298	260	180	18	171	4
2.56	123	248	117	0.47	0.16311	0.00320	9.50114	0.25344	0.42242	0.00911	2488	20	2388	25	2271	41
2.57	17	481	440	0.91	0.04977	0.00138	0.19980	0.00656	0.02911	0.00064	184	39	185	6	185	4
2.58	13	395	426	1.08	0.04924	0.00145	0.17141	0.00585	0.02524	0.00056	159	41	161	5	161	4
2.59	3	105	66	0.63	0.05057	0.00371	0.16308	0.01217	0.02338	0.00058	221	124	153	11	149	4
2.60	5	141	203	1.45	0.04914	0.00319	0.16370	0.01096	0.02416	0.00056	155	109	154	10	154	4
3.1	6	158	201	1.27	0.04984	0.00210	0.19857	0.00837	0.02889	0.00052	188	65	184	7	184	3
3.2	4	101	165	1.63	0.04959	0.00209	0.18688	0.00787	0.02733	0.00050	176	64	174	7	174	3
3.3	42	65	78	1.21	0.16604	0.00291	11.52751	0.22790	0.50343	0.00783	2518	15	2567	18	2629	34
3.4	152	267	221	0.83	0.16716	0.00280	10.80322	0.20772	0.46865	0.00715	2529	15	2506	18	2478	31
3.5	158	385	114	0.30	0.16071	0.00270	8.35425	0.16098	0.37696	0.00575	2463	15	2270	17	2062	27
3.6	3	85	109	1.28	0.04972	0.00266	0.19842	0.01043	0.02894	0.00059	182	84	184	9	184	4
3.7	44	66	79	1.19	0.16772	0.00298	12.03349	0.24045	0.52027	0.00812	2535	15	2607	19	2700	34
3.8	6	129	96	0.74	0.04944	0.00363	0.17603	0.01283	0.02582	0.00051	169	128	165	11	164	3
3.9	6	176	170	0.96	0.05346	0.00288	0.19497	0.01045	0.02644	0.00050	348	87	181	9	168	3
3.10	2	78	94	1.20	0.06170	0.00673	0.17528	0.01902	0.02060	0.00044	664	200	164	16	131	3
3.11	137	280	189	0.67	0.16831	0.00294	9.64981	0.19085	0.41576	0.00641	2541	15	2402	18	2241	29
3.12	129	241	164	0.68	0.16723	0.00291	10.48381	0.20693	0.45460	0.00699	2530	15	2478	18	2416	31
3.13	8	230	199	0.86	0.04984	0.00183	0.19668	0.00725	0.02861	0.00051	188	53	182	6	182	3
3.14	62	120	51	0.43	0.16678	0.00298	10.57864	0.21260	0.45996	0.00713	2526	16	2487	19	2439	31
3.15	3	128	204	1.59	0.04859	0.00298	0.13412	0.00817	0.02001	0.00039	128	101	128	7	128	2
3.16	11	236	670	2.84	0.04956	0.00186	0.18840	0.00710	0.02757	0.00048	174	56	175	6	175	3
3.17	11	301	531	1.76	0.04954	0.00153	0.18538	0.00585	0.02713	0.00046	173	43	173	5	173	3
3.18	7	187	312	1.67	0.04960	0.00254	0.19811	0.01008	0.02897	0.00055	176	83	184	9	184	3
3.19	2	88	89	1.01	0.04861	0.00344	0.13551	0.00933	0.01992	0.00042	129	117	127	8	127	3
3.20	2	94	126	1.34	0.04868	0.00360	0.13364	0.00976	0.01991	0.00043	132	123	127	9	127	3
3.21	2	44	69	1.56	0.04964	0.00431	0.19089	0.01634	0.02788	0.00066	178	149	177	14	177	4
3.22	5	160	120	0.75	0.04937	0.00285	0.18926	0.01087	0.02780	0.00053	165	96	176	9	177	3
3.23	3	119	79	0.66	0.05613	0.00448	0.14674	0.01155	0.01896	0.00042	458	136	139	10	121	3
3.24	117	215	165	0.77	0.16414	0.00302	10.26016	0.21071	0.45327	0.00702	2499	16	2459	19	2410	31
3.25	136	237	192	0.81	0.16860	0.00311	11.02632	0.22655	0.47425	0.00734	2544	16	2525	19	2502	32
3.26	4	143	113	0.79	0.04960	0.00236	0.18467	0.00869	0.02700	0.00052	176	74	172	7	172	3
3.27	97	153	235	1.54	0.16776	0.00315	10.74834	0.22386	0.46460	0.00724	2535	17	2502	19	2460	32
3.28	10	262	537	2.05	0.04954	0.00179	0.18266	0.00660	0.02674	0.00048	173	51	170	6	170	3
3.29	3	133	148	1.11	0.04860	0.00444	0.13361	0.01212	0.01993	0.00042	129	163	127	11	127	3
3.30	2	55	20	0.36	0.06062	0.00673	0.23108	0.02550	0.02764	0.00060	626	204	211	21	176	4
3.32	7	282	396	1.40	0.04849	0.00182	0.13349	0.00502	0.01996	0.00036	123	55	127	4	127	2
3.33	59	97	97	1.00	0.16656	0.00327	11.03526	0.23714	0.48046	0.00756	2523	17	2526	20	2529	33
3.34	5	143	111	0.78	0.05021	0.00588	0.17522	0.02021	0.02531	0.00053	205	261	164	17	161	3
3.35	6	206	171	0.83	0.04938	0.00217	0.18397	0.00810	0.02702	0.00048	166	70	171	7	172	3
4.1	1	20	32	1.58	0.04942	0.01024	0.17304	0.03576	0.02539	0.00086	168	329	162	31	162	5
4.2	1	27	11	0.42	0.04938	0.01090	0.17421	0.03841	0.02558	0.00083	166	354	163	33	163	5
4.3	111	209	91	0.44	0.16792	0.00246	10.23314	0.25493	0.44187	0.01000	2537	19	2456	23	2359	45
4.4	59	93	70	0.75	0.17168	0.00258	11.54545	0.29002	0.48762	0.01108	2574	19	2568	23	2560	48
4.5	3	28	86	3.08	0.04605	0.00782	0.14611	0.02447	0.02301	0.00065	–	–	138	22	147	4
4.6	122	305	96	0.31	0.16108	0.00237	7.55749	0.18830	0.34019	0.00769	2467	19	2180	22	1888	37
4.7	90	166	86	0.52	0.16590	0.00247	10.03463	0.25089	0.43858	0.00993	2517	19	2438	23	2344	44
4.8	3	90	50	0.56	0.04969	0.00388	0.19452	0.01557	0.02839	0.00070	181	135	180	13	180	4
4.9	2	70	39	0.56	0.04605	0.00335	0.12227	0.00835	0.01926	0.00048	–	–	117	8	123	3
4.11	5	255	110	0.43	0.04835	0.00271	0.12170	0.00716	0.01825	0.00044	116	89	117	6	117	3
4.12	3	84	91	1.08	0.04946	0.00384	0.17902	0.01420	0.02625	0.00066	170	132	167	12	167	4
4.13	77	135	91	0.67	0.16472	0.00258	10.11628	0.25567	0.44535	0.01007	2505	19	2445	23	2375	45
4.14	2	58	50	0.86	0.04923	0.00617	0.16735	0.02110	0.02465	0.00067	159	229	157	18</		

Table 1 (continued)

Spot	Concentrations (ppm)			Th/U	Isotopic ratios						Isotopic ages (Ma)						
	Pb	U	Th		$^{207}\text{Pb}/^{206}\text{Pb}^a$	$\pm 1\sigma$	$^{207}\text{Pb}/^{235}\text{U}$	$\pm 1\sigma$	$^{206}\text{Pb}/^{238}\text{U}$	$\pm 1\sigma$	$^{207}\text{Pb}/^{206}\text{Pb}$	$\pm 1\sigma$	$^{207}\text{Pb}/^{235}\text{U}$	$\pm 1\sigma$	$^{206}\text{Pb}/^{238}\text{U}$	$\pm 1\sigma$	
12XTM01																	
4.24	10	331	639	1.93	0.04856	0.00188	0.13178	0.00565	0.01968	0.00046	127	58	126	5	126	3	
4.26	160	220	519	2.36	0.16570	0.00295	9.70157	0.25489	0.42456	0.00958	2515	20	2407	24	2281	43	
4.27	9	247	322	1.30	0.06129	0.00658	0.21466	0.02231	0.02540	0.00069	650	241	197	19	162	4	
4.29	3	95	113	1.19	0.06469	0.00431	0.24128	0.01648	0.02705	0.00069	764	101	219	13	172	4	
4.31	74	120	121	1.01	0.16492	0.00320	10.27548	0.27915	0.45181	0.01026	2507	21	2460	25	2403	46	
4.32	18	540	589	1.09	0.05042	0.00144	0.17313	0.00587	0.02490	0.00057	214	39	162	5	159	4	
4.33	3	92	77	0.83	0.04954	0.00395	0.18911	0.01535	0.02768	0.00070	173	136	176	13	176	4	
4.34	5	163	105	0.64	0.04922	0.00224	0.16865	0.00820	0.02485	0.00060	158	69	158	7	158	4	
4.35	8	203	398	1.96	0.06097	0.00258	0.22284	0.01016	0.02650	0.00064	638	57	204	8	169	4	
4.36	13	258	567	2.20	0.04605	0.00349	0.18818	0.01354	0.02964	0.00071	–	–	175	12	188	4	
4.38	1	31	30	0.96	0.04855	0.01279	0.13467	0.03540	0.02011	0.00068	126	406	128	32	128	4	
4.39	8	267	454	1.70	0.04852	0.00242	0.13126	0.00691	0.01962	0.00047	125	77	125	6	125	3	
4.40	8	247	224	0.91	0.04919	0.00235	0.16706	0.00846	0.02463	0.00059	157	74	157	7	157	4	
4.41	50	83	81	0.98	0.16405	0.00354	10.10482	0.28719	0.44663	0.01019	2498	22	2444	26	2380	45	
4.42	7	194	222	1.14	0.04926	0.00283	0.17250	0.01026	0.02539	0.00063	160	91	162	9	162	4	

^a Corrected ratios.

by SHRIMP yield similar age patterns as those done by LA-ICP-MS (see details in the Appendix).

4.2. Bulk rock geochemistry

The Xintaimen rhyolite samples have relatively high SiO₂ and K₂O/Na₂O (0.59–0.97) and mostly plot in the rhyolite field on the TAS diagram, except for sample 11XC11 which has the lowest SiO₂ content and lies in the trachydacite field (Table 2; Fig. 4). These samples are all metaluminous (Table 2) and show enrichment of LREEs over HREEs without obvious Eu anomalies (Fig. 5a). In the primitive mantle-normalized trace element diagram (Fig. 5b), they are relatively enriched in large ion lithophile elements (LILEs), with limited variation, and depleted in some high field strength elements (HFSEs; but without Zr or Hf depletion). They are characterized by positive Sr anomalies with high Sr/Y ratios of 90–129 (Table 2; Fig. 5b). They have relatively low compatible element abundances (e.g., Cr and Ni; Table 2). These samples display a narrow range of initial $^{87}\text{Sr}/^{86}\text{Sr}$ ratios (0.705682–0.706067) and highly negative $\epsilon_{\text{Nd}}(t)$ values (−16.6 to −14.4) with two-stage depleted mantle Nd model ages (T_{DM2} ages) of 2266–2087 Ma, when calculated at 125 Ma (Table 3; Fig. 6).

4.3. In situ zircon Hf-O isotopes

The Neoarchean to Early Paleoproterozoic mafic lower crust heated by mantle-derived melts

The Xintaimen rhyolite has high Sr/Y and (La/Yb)_N ratios (Figs. 5 and 9), but is also characterized by relatively high K₂O/Na₂O ratios

(all >0.5) (Fig. 4b), distinct from typical young slab-derived sodic modern adakites (Defant and Drummond, 1990; Martin et al., 2005) but similar to lower crust-derived potassic ‘adakitic rocks’ (Atherton and Petford, 1993; Xiao and Clemens, 2007).

The Xintaimen adakitic rhyolite is similar to typical TTGs and adakites and experimental metabasalt melts in terms of major and trace elements (Figs. 4, 5 and 9). The high SiO₂ and low MgO of the Xintaimen rhyolite are also similar to high-silica adakites as proposed by Martin et al. (2005) (Fig. 9c), which experienced limited or no interaction with a mantle wedge. Their enriched Sr-Nd isotopic compositions (Fig. 6) and relatively low abundances of compatible elements (e.g., Cr and Ni; Fig. 9d) contrast these rocks with the Jurassic Xinglonggou lavas from eastern China (Gao et al., 2004), which are interpreted as the result of foundering of mafic lower crust into, and interacting with, underlying convective mantle. Thus, the primary magmas parental to the Xintaimen rhyolite show little evidence for significant interaction with mantle peridotite. Furthermore, the bulk rock Nd T_{DM2} ages (2266–2087 Ma), and Hf T_{DM2} ages (2225–1315 Ma) and $\delta^{18}\text{O}$ values of 5.56–5.75‰ (close to mantle-zircon values 5.3 ± 0.3‰; Table 5; Fig. 8b; Valley, 2003) of the Early Cretaceous magmatic zircons, together are best interpreted as reflecting generation by melting of ancient mafic lower crust.

Recently, many Mesozoic lower crust-derived rocks have been reported from the NCC (e.g., Gao et al., 2004; Jiang et al., 2007; Ma et al., 2012; Wang et al., 2015), with heterogeneous lower crustal sources inferred from their highly variable Sr-Nd isotopic compositions (Fig. 6). The bulk rock Nd isotope composition of the Xintaimen rhyolite seems to be distinct from Archean lower crust, sampled from exposed Archean terrain granulites and amphibolites (Fig. 6b). It is, however, comparable to that of the Late Triassic Taili adakitic plutons from the same area (Fig. 7a; Wang et al., 2015), whose source is believed to be mantle plume-related mafic rocks generated during Paleoproterozoic intracontinental extension and rifting of the NCC (Peng et al., 2012). We suggest that the bulk rock Nd T_{DM2} ages of the Xintaimen rhyolite (2266–2087 Ma), as well as data from the two Early Cretaceous zircons with Paleoproterozoic Hf T_{DM2} ages (Table 4; #2.1, $T_{\text{DM2}} = 2225$ Ma; #2.32, $T_{\text{DM2}} = 2010$ Ma) extracted from the rhyolite, imply that the lower crustal source of the rhyolite could have been mafic rocks that underplated the base of the NCC Archean crust during the Paleoproterozoic (2.3–2.0 Ga).

Melting of lower crust is commonly triggered by excess heat supplied by contemporaneous emplacement of mantle-derived mafic melts (e.g., Atherton and Petford, 1993; Huppert and Sparks, 1988; Ma et al., 2016; Niu, 2005). In the Early Cretaceous, the NCC was characterized by an extremely high geothermal gradient (>90 mW/m² vs.

Table 2

Bulk rock major and trace element data for the Xintaimen rhyolite.

Samples	11XC10	11XC11	11XC12	12XTM03	12XTM04	12XTM05	12XTM06	12XTM07	12XTM08	12XTM09	12XTM10	12XTM12
<i>Major elements (wt%)</i>												
SiO ₂	68.25	65.59	67.99	70.36	69.61	69.43	70.32	69.22	68.76	70.32	70.34	68.99
TiO ₂	0.41	0.44	0.40	0.32	0.34	0.35	0.32	0.35	0.34	0.32	0.33	0.35
Al ₂ O ₃	13.17	14.50	13.44	13.13	13.04	13.65	13.23	13.33	13.36	12.91	12.86	13.19
Fe ₂ O _{3T}	3.23	3.62	3.30	2.76	2.78	2.92	2.77	2.99	2.77	2.79	2.76	2.90
MnO	0.05	0.05	0.05	0.04	0.04	0.04	0.04	0.05	0.04	0.04	0.04	0.04
MgO	1.36	1.46	1.40	1.19	1.19	1.27	1.19	1.22	1.34	1.19	1.21	1.23
CaO	3.09	3.32	3.05	2.90	3.16	2.95	2.99	3.02	3.08	2.91	2.98	3.08
Na ₂ O	4.19	4.47	4.14	3.46	3.11	3.81	3.54	3.91	3.21	3.33	3.41	3.29
K ₂ O	2.91	3.35	2.96	2.45	2.57	2.33	2.28	2.32	2.47	2.64	2.30	3.20
P ₂ O ₅	0.17	0.19	0.18	0.14	0.16	0.15	0.15	0.16	0.15	0.14	0.15	0.16
LOI	2.36	2.21	2.29	3.09	3.83	2.96	3.01	3.27	4.35	3.23	3.47	3.40
Total	99.20	99.21	99.20	99.85	99.84	99.85	99.85	99.84	99.86	99.84	99.83	99.83
K ₂ O/Na ₂ O	0.69	0.75	0.71	0.71	0.83	0.61	0.64	0.59	0.77	0.79	0.67	0.97
A/CNK	0.84	0.85	0.86	0.96	0.96	0.97	0.96	0.92	0.99	0.95	0.95	0.91
Mg#	49.6	48.6	49.7	50.2	49.9	50.3	50.0	48.7	52.9	49.8	50.4	49.6
<i>Trace elements (ppm)</i>												
Li	7.48	7.18	7.54	19.99	20.94	18.37	14.56	17.28	29.50	21.06	20.84	20.94
P	748	753	771	1155	1264	1191	1181	1206	1245	1151	1215	1197
K	25,640	27,020	26,767	39,600	41,400	36,300	35,820	37,180	41,500	42,880	38,740	47,960
Sc	4.72	4.73	4.84	6.80	6.72	6.75	6.83	6.65	7.17	6.63	6.89	6.83
Ti	2902	2894	2913	3090	3418	3226	3160	3324	3414	3112	3310	3212
V	42.20	42.04	43.47	55.14	60.82	59.28	55.86	61.02	62.84	56.40	59.62	59.42
Cr	29.40	36.34	31.77	37.48	37.84	51.82	42.72	38.86	43.86	36.58	39.40	37.02
Mn	306	316	321	447	451	465	450	497	458	457	468	479
Co	5.95	5.97	5.98	8.76	9.44	9.27	9.00	9.38	9.46	9.08	9.42	8.97
Ni	11.35	14.15	12.86	18.59	18.55	24.10	21.80	18.08	19.96	17.91	18.32	17.44
Cu	13.54	13.75	13.27	20.76	21.84	22.02	21.98	22.06	21.92	20.84	22.14	22.20
Zn	44.76	47.58	46.06	65.50	71.48	71.06	66.52	68.52	68.90	65.78	70.30	67.32
Ga	16.24	16.33	16.65	21.24	22.98	21.46	21.48	21.52	22.22	21.04	22.02	21.36
Rb	107	106	107	117	78	116	100	113	70	110	103	105
Sr	693	659	712	791	1006	745	865	763	763	773	816	810
Y	7.33	7.29	7.56	7.59	7.82	7.48	7.62	7.41	7.66	7.34	7.57	7.34
Zr	229	227	235	188	204	196	190	196	203	188	199	197
Hf	4.48	4.44	4.61	4.27	4.66	4.48	4.26	4.50	4.53	4.23	4.49	4.47
Nb	14.11	14.09	14.46	10.56	11.82	11.18	10.81	11.76	11.41	10.52	11.20	11.04
Ta	1.45	1.74	1.38	0.66	0.68	0.71	0.65	0.72	0.69	0.70	0.72	0.62
Cs	6.79	3.06	4.73	8.40	9.51	2.81	6.35	4.38	1.72	7.86	6.45	5.50
Ba	1232	1219	1282	1182	1289	1144	1162	1113	1128	1147	1162	1142
La	35.46	35.44	36.50	35.02	36.68	35.10	34.94	33.70	34.80	33.80	34.80	34.08
Ce	62.60	62.74	64.43	62.98	65.86	63.00	62.28	61.06	62.80	61.10	62.86	61.76
Pr	6.49	6.54	6.71	6.52	6.85	6.54	6.49	6.26	6.56	6.36	6.50	6.37
Nd	22.10	22.24	22.76	21.08	21.98	21.22	20.84	20.30	21.08	20.42	20.92	20.48
Sm	3.26	3.28	3.34	3.14	3.20	3.09	3.10	2.98	3.09	3.00	3.06	2.99
Eu	0.94	0.95	0.97	0.94	0.99	0.94	0.92	0.91	0.95	0.91	0.92	0.92
Gd	2.45	2.47	2.52	2.39	2.48	2.38	2.36	2.27	2.41	2.29	2.36	2.28
Tb	0.28	0.28	0.29	0.27	0.28	0.27	0.27	0.26	0.27	0.26	0.26	0.26
Dy	1.41	1.42	1.47	1.33	1.40	1.32	1.31	1.29	1.34	1.29	1.32	1.29
Ho	0.26	0.26	0.26	0.25	0.26	0.25	0.24	0.24	0.25	0.24	0.24	0.24
Er	0.71	0.70	0.74	0.67	0.69	0.66	0.66	0.64	0.67	0.65	0.66	0.64
Tm	0.10	0.10	0.10	0.09	0.09	0.09	0.09	0.09	0.09	0.09	0.09	0.09
Yb	0.63	0.63	0.65	0.59	0.60	0.58	0.59	0.58	0.59	0.57	0.58	0.58
Lu	0.09	0.09	0.10	0.09	0.09	0.09	0.09	0.09	0.09	0.08	0.09	0.09
Pb	13.94	14.16	14.09	11.34	10.75	11.52	11.35	11.65	11.71	11.01	11.47	11.46
Th	6.16	6.20	6.35	4.98	5.10	4.96	4.93	4.79	5.04	4.77	4.91	4.84
U	1.16	1.18	1.19	0.77	0.95	0.77	0.77	0.78	0.75	0.79	0.77	
ΣREE	136.8	137.1	140.8	135.4	141.4	135.5	134.2	130.7	135.0	131.1	134.7	132.1
Eu/Eu*	0.97	0.98	0.98	1.01	1.04	1.02	1.01	1.03	1.02	1.02	1.01	1.04
(La/Yb) _N	40	40	40	42	44	43	43	42	43	43	42	
Sr/Y	94	90	94	104	129	100	114	103	100	105	108	110

Mg# = molar 100 * Mg / (Mg + Fe).

~40 mW/m² in the Paleozoic; Ma et al., 2016; Zheng et al., 2006), associated with the generation of large volumes of igneous rocks derived through melting of ancient lower crust (Niu et al., 2015; S.-H. Zhang et al., 2014). The presence of a mantle-derived mafic underplating at this time is also inferred from the existence of widespread and broadly contemporaneous alkaline rocks and basalts in the NCC (Gao et al., 2008; Zhang et al., 2010; S.-H. Zhang et al., 2014). Mafic magmatic enclaves are very common in the Early Cretaceous granites of the NCC

(e.g., Chen et al., 2009). These granites are characterized by bulk rock $\varepsilon_{\text{Nd}}(t)$ and zircon $\varepsilon_{\text{Hf}}(t)$ values (S.-H. Zhang et al., 2014) that, although highly variable, typically lie within a range consistent with a significant mantle contribution to the magmatism in terms of both material and (hence) heat (e.g., Chen et al., 2004; Ma et al., 2016). Therefore, we propose that during the Early Cretaceous, extensive heat, related to mantle-derived mafic melts that accumulated beneath the NCC crust, caused the Paleoproterozoic mafic lower crust to undergo extensive

Table 3

Bulk rock Nd isotopic compositions of the Xintaimen rhyolite.

Sample	Rb (ppm)	Sr (ppm)	$^{87}\text{Rb}/^{86}\text{Sr}$	$^{87}\text{Sr}/^{86}\text{Sr}$	$\pm 2\sigma$	$I_{\text{Sr}}(t)$	Sm (ppm)	Nd (ppm)	$^{147}\text{Sm}/^{144}\text{Nd}$	$^{143}\text{Nd}/^{144}\text{Nd}$	$\pm 2\sigma$	$\varepsilon_{\text{Nd}}(0)$	$(^{143}\text{Nd}/^{144}\text{Nd})_i^{\text{a}}$	$\varepsilon_{\text{Nd}}(t)$	T_{DM1} (Ma)	T_{DM2} (Ma)	$f^{\text{Sm/Nd}}$
12XTM03	117	791	0.418	0.706608	4	0.705866	3.14	21.08	0.095	0.511723	2	-17.8	0.511646	-16.2	1819	2236	-0.52
12XTM04	78	1006	0.218	0.706454	6	0.706067	3.20	21.98	0.092	0.511720	2	-17.9	0.511644	-16.2	1792	2239	-0.53
12XTM05	116	745	0.438	0.706706	5	0.705927	3.09	21.22	0.092	0.511703	6	-18.2	0.511627	-16.6	1813	2266	-0.53
12XTM08	70	763	0.259	0.706518	2	0.706059	3.09	21.08	0.093	0.511720	2	-17.9	0.511643	-16.3	1802	2240	-0.53
12XTM10	103	816	0.357	0.706317	9	0.705682	3.06	20.92	0.093	0.511816	11	-16.0	0.511740	-14.4	1678	2087	-0.53
11XC10	107	693	0.437	0.706652	6	0.705875	3.26	22.10	0.094	0.511721	1	-17.9	0.511644	-16.3	1810	2239	-0.52
11XC11	106	659	0.454	0.706727	7	0.705921	3.28	22.24	0.094	0.511724	2	-17.8	0.511647	-16.2	1805	2234	-0.52
11XC12	107	712	0.424	0.706730	8	0.705976	3.34	22.76	0.093	0.511720	2	-17.9	0.511644	-16.2	1801	2239	-0.53

Parameters used in the calculation are as follows: ^{87}Rb decay $\lambda = 1.42 \times 10^{-11} \text{ year}^{-1}$; ^{147}Sm decay $\lambda = 6.54 \times 10^{-12} \text{ year}^{-1}$; $(^{147}\text{Sm}/^{144}\text{Nd})_{\text{CHUR}} = 0.1967$, $(^{143}\text{Nd}/^{144}\text{Nd})_{\text{CHUR}} = 0.512638$; $(^{147}\text{Sm}/^{144}\text{Nd})_{\text{DM}} = 0.2137$, $(^{143}\text{Nd}/^{144}\text{Nd})_{\text{DM}} = 0.51315$.

^a Calculated at 125 Ma.

melting, generating magmas parental to the Xintaimen rhyolite. The mantle-derived mafic melts could have modified magma compositions to some degrees, reflected by the relatively large variations of Hf isotopic compositions of the Early Cretaceous and Jurassic zircons (Table 4; Fig. 7).

As discussed above, the Xintaimen rhyolite possibly share the same Paleoproterozoic mafic lower crustal source as the nearby Late Triassic Taili adakitic plutons. According to Wang et al. (2015), the Taili adakitic rocks formed during melting at 10–12 kbar and 780–820 °C. The Xintaimen rhyolite has slightly less fractionated REE patterns (lower $(\text{La/Yb})_N$ ratios) and slightly lower Sr/Y ratios (Figs. 5, 9a and b) than the Taili adakitic plutons, suggesting lower pressure melting (i.e. indicative of lower garnet abundances and higher plagioclase/garnet ratios in the melt residuals; Moyen, 2009), but, nevertheless, probably still within the range of 10–12 kbar.

5.2. Magmatic process inferred by zircon geochronology

Because of the presence of famous Jehol biota in the Yixian Formation, the age of this formation has been well constrained by both U-Pb and $^{40}\text{Ar}-^{39}\text{Ar}$ methods to the period 126–120 Ma (e.g., Swisher et al., 2002; Yang et al., 2007). Our *in situ* zircon U-Pb dating of the Xintaimen rhyolite shows that they contain three groups of zircons with contrasting ages (Table 1 and Fig. 3) and the youngest group yields a weighted mean $^{206}\text{Pb}/^{238}\text{U}$ age of 125.4 ± 2.2 Ma (2σ , MSWD = 1.8), which should represent the eruption time of the Xintaimen rhyolite.

The Neoarchean to Early Paleoproterozoic zircons within the Xintaimen rhyolite are xenocrysts captured by the magmas en route to the surface, rather than inherited zircons from the mafic lower crustal source of the adakitic rhyolite. Evidence for this is that: (1) in CL images, they show perfect oscillatory growth zoning of felsic magma affinity, and have no overgrowth rims or melt-corroded textures (Fig. 3a); and (2) their Hf isotopic compositions are distinct from those of the Early Cretaceous zircons, but similar to those of the Neoarchean basement rocks (Fig. 7a; Wang et al., 2016).

The Xintaimen rhyolite also contains abundant Jurassic zircons with successive and concordant U-Pb ages (193–146 Ma). They have no overgrowth rims and show internal textures similar to those of the Early Cretaceous zircons on CL images (Fig. 3a). They also share similar Hf isotopic compositions with the Early Cretaceous zircons (Fig. 7b). It appears as if these Jurassic zircons crystallized from the same parental magmas as those of the Early Cretaceous zircons. However, it is hard to imagine that a magma chamber can last from 193 Ma to 117 Ma, ~70 Myrs with a gap of ~15 Myrs (between 146 Ma and 131 Ma). Jurassic igneous rocks are widespread in the study area (Fig. 1), with various lithologies including basaltic-andesitic-rhyolitic volcanic rocks, mafic dykes and granitic plutons (Wu et al., 2006; X. Zhang et al., 2014). Thus, these Jurassic zircons

should be also xenocrysts captured by the rhyolitic magmas en route to the surface.

The relatively enriched Hf isotopic compositions of all the Jurassic zircons in the Xintaimen rhyolite clearly point to a genetic connection with ancient crustal materials, in common with the zircons from the Jurassic ancient lower crust-derived igneous rocks in the study area (Table 4; Fig. 7; X. Zhang et al., 2014). These zircons also have $\delta^{18}\text{O}$ values of 5.65–6.67‰ (Table 5; Fig. 8), indicating derivation of their parental magmas from sources with little, if any, contribution from supracrustal components (Eiler, 2001). Recent Sr-Nd-Hf isotope studies of the Jurassic igneous rocks in western Liaoning imply the involvement of ancient lower crust via complex crust-mantle interaction (e.g., foundering of mafic lower continental crust into underlying convecting mantle, or underplating of mafic magmas, with subsequent interaction with lower crust; Gao et al., 2004; Yang and Li, 2008; X. Zhang et al., 2014). A comprehensive summary of geochemical data on Jurassic igneous rocks from the NCC shows that most of them were sourced from ancient lower crust (S.-H. Zhang et al., 2014). Nevertheless, combined with previous studies of the Jurassic magmatism in western Liaoning and the NCC, it can be deduced that the ancient lower crust participated in the formation of the parental magmas from which these Jurassic xenocrystic zircons were crystallized.

It is noteworthy, however, that the Early Cretaceous zircons only constitute a minor portion (14 grains) among the whole population (167 grains) of the dated zircons from the Xintaimen rhyolite, compared with the Neoarchean to Early Paleoproterozoic- and Jurassic-aged xenocrystic zircons (Fig. 3). One plausible explanation for this observation is that the Early Cretaceous magma chamber developed within crust dominated by Jurassic plutonic rocks and Neoarchean basement rocks. Compared to deep-seated felsic intrusions, the erupted rhyolitic magmas ascended and cooled too rapidly to allow sufficient growth of new zircons. The Early Cretaceous rhyolitic magmas would have formed only a few 'phenocrystic' zircons, but captured and inherited many xenocrystic zircons.

5.3. Long-lived melting of the ancient lower crust beneath the NCC in response to paleo-Pacific plate subduction

The Hf-O isotopic compositions of the Early Cretaceous magmatic zircons and the bulk rock Nd isotopic compositions of the Xintaimen rhyolite indicate derivation from partial melting of the Paleoproterozoic mafic lower crust. The Hf-O isotopic compositions of the Jurassic xenocrystic zircons, also suggest that their parental melts were derived from ancient lower crust. Therefore, the Xintaimen adakitic rhyolite records, in its primary and xenocrystic zircon cargo, a long-lived (~70 Myrs) melting process of the ancient lower crust beneath the NCC.

Table 4*In situ* zircon Hf isotopic compositions of the Xintaimen rhyolite.

Spot	<i>t</i> (Ma)	$^{176}\text{Yb}/^{177}\text{Hf}$	$\pm 2\sigma$	$^{176}\text{Lu}/^{177}\text{Hf}$	$\pm 2\sigma$	$^{176}\text{Hf}/^{177}\text{Hf}$	$\pm 2\sigma$	$(^{176}\text{Hf}/^{177}\text{Hf})_i^{\text{a}}$	$\epsilon_{\text{Hf}}(0)$	$\epsilon_{\text{Hf}}(t)$	T_{DM1} (Ma)	T_{DM2} (Ma)	$f_{\text{Lu/Hf}}$
<i>12XTM01</i>													
1.1	158	0.040989	0.000583	0.001445	0.000020	0.282375	0.000019	0.282371	-14.0	-10.7	1253	1549	-0.96
1.2	174	0.048696	0.000384	0.001644	0.000012	0.282417	0.000020	0.282411	-12.6	-8.9	1201	1471	-0.95
1.3	153	0.040135	0.000654	0.001156	0.000016	0.282181	0.000019	0.282178	-20.9	-17.7	1515	1896	-0.97
1.4	2565	0.020931	0.000349	0.000737	0.000011	0.281331	0.000020	0.281295	-51.0	5.4	2662	2691	-0.98
1.5	177	0.039587	0.000354	0.001439	0.000008	0.282406	0.000018	0.282401	-13.0	-9.2	1210	1488	-0.96
1.6	146	0.019785	0.000063	0.000709	0.000004	0.282224	0.000023	0.282222	-19.4	-16.3	1439	1820	-0.98
1.7	153	0.042696	0.001213	0.001420	0.000045	0.282204	0.000022	0.282200	-20.1	-16.9	1494	1857	-0.96
1.8	2576	0.030727	0.001214	0.001171	0.000049	0.281321	0.000015	0.281264	-51.3	4.5	2705	2741	-0.96
1.9	166	0.066101	0.000267	0.002258	0.000004	0.282116	0.000017	0.282109	-23.2	-19.8	1655	2015	-0.93
1.10	163	0.028046	0.000837	0.000909	0.000028	0.282167	0.000015	0.282164	-21.4	-17.9	1526	1919	-0.97
1.11	171	0.013332	0.000096	0.000442	0.000002	0.282073	0.000022	0.282071	-24.7	-21.0	1636	2082	-0.99
1.12	168	0.041408	0.000206	0.001379	0.000006	0.282219	0.000017	0.282214	-19.6	-16.0	1472	1826	-0.96
1.13	175	0.018648	0.000149	0.000628	0.000006	0.282244	0.000014	0.282242	-18.7	-14.9	1408	1776	-0.98
1.14	191	0.024560	0.000455	0.000893	0.000016	0.282134	0.000018	0.282131	-22.5	-18.5	1570	1968	-0.97
1.15	2549	0.016847	0.000129	0.000599	0.000004	0.281280	0.000016	0.281251	-52.7	3.5	2720	2772	-0.98
2.1	127	0.014786	0.000064	0.000376	0.000003	0.282000	0.000027	0.281999	-27.3	-24.6	1733	2225	-0.99
2.2	177	0.072409	0.000624	0.001767	0.000017	0.282326	0.000026	0.282320	-15.8	-12.1	1334	1633	-0.95
2.3	181	0.054376	0.000194	0.001430	0.000011	0.282373	0.000021	0.282369	-14.1	-10.3	1255	1546	-0.96
2.4	178	0.060106	0.000478	0.001648	0.000008	0.282435	0.000020	0.282430	-11.9	-8.2	1174	1436	-0.95
2.5	2489	0.017751	0.000075	0.000457	0.000005	0.281307	0.000023	0.281285	-51.8	3.3	2676	2732	-0.99
2.7	159	0.035684	0.000175	0.000844	0.000007	0.282195	0.000030	0.282193	-20.4	-17.0	1483	1868	-0.97
2.8	150	0.044759	0.000132	0.000962	0.000008	0.282185	0.000027	0.282182	-20.8	-17.6	1503	1890	-0.97
2.9	2542	0.062958	0.000817	0.001456	0.000023	0.281334	0.000029	0.281263	-50.9	3.7	2708	2753	-0.96
2.10	2534	0.027229	0.000062	0.000641	0.000004	0.281314	0.000029	0.281283	-51.6	4.2	2679	2722	-0.98
2.11	163	0.090729	0.000831	0.001840	0.000010	0.282264	0.000027	0.282258	-18.0	-14.6	1426	1749	-0.94
2.12	167	0.058948	0.001057	0.001290	0.000027	0.282267	0.000024	0.282263	-17.9	-14.3	1401	1740	-0.96
2.13	175	0.047712	0.000825	0.001153	0.000014	0.282406	0.000028	0.282403	-12.9	-9.2	1200	1486	-0.97
2.14	2496	0.008878	0.000705	0.000167	0.000015	0.281191	0.000024	0.281183	-55.9	-0.2	2810	2908	-0.99
2.15	161	0.028528	0.000619	0.000624	0.000011	0.282178	0.000024	0.282177	-21.0	-17.5	1498	1897	-0.98
2.16	193	0.072250	0.000797	0.001972	0.000017	0.282362	0.000023	0.282355	-14.5	-10.5	1290	1566	-0.94
2.17	162	0.050571	0.000603	0.001041	0.000015	0.282232	0.000025	0.282229	-19.1	-15.6	1439	1802	-0.97
2.18	189	0.056242	0.001760	0.001386	0.000041	0.282413	0.000028	0.282408	-12.7	-8.7	1198	1472	-0.96
2.19	169	0.046889	0.000209	0.001029	0.000005	0.282180	0.000023	0.282177	-20.9	-17.3	1512	1893	-0.97
2.20	173	0.073981	0.000789	0.001469	0.000021	0.282183	0.000027	0.282178	-20.8	-17.2	1525	1889	-0.96
2.21	2513	0.028858	0.000221	0.000704	0.000004	0.281253	0.000023	0.281219	-53.7	1.5	2766	2840	-0.98
2.22	191	0.085071	0.001287	0.001936	0.000019	0.282173	0.000028	0.282166	-21.2	-17.2	1559	1905	-0.94
2.25	2543	0.028915	0.000809	0.000724	0.000014	0.281374	0.000027	0.281339	-49.4	6.5	2602	2620	-0.98
2.26	192	0.074340	0.000451	0.001909	0.000008	0.282395	0.000026	0.282388	-13.3	-9.4	1240	1506	-0.94
2.27	167	0.047375	0.000175	0.000972	0.000006	0.282198	0.000025	0.282194	-20.3	-16.8	1485	1862	-0.97
2.28	163	0.040105	0.000379	0.000818	0.000004	0.282282	0.000024	0.282280	-17.3	-13.8	1362	1711	-0.98
2.29	167	0.061030	0.000613	0.001290	0.000019	0.282184	0.000024	0.282180	-20.8	-17.3	1517	1888	-0.96
2.30	162	0.048552	0.000678	0.001056	0.000011	0.282236	0.000027	0.282233	-19.0	-15.5	1435	1795	-0.97
2.31	168	0.039583	0.000358	0.000861	0.000010	0.282340	0.000025	0.282338	-15.3	-11.7	1283	1606	-0.97
2.32	118	0.056943	0.000530	0.001523	0.000029	0.282124	0.000030	0.282120	-22.9	-20.5	1611	2010	-0.95
2.33	2522	0.039630	0.000544	0.000999	0.000010	0.281209	0.000027	0.281160	-55.3	-0.4	2846	2939	-0.97
2.34	2482	0.017292	0.000422	0.000424	0.000007	0.281207	0.000021	0.281187	-55.3	-0.4	2806	2905	-0.99
2.35	167	0.039042	0.000231	0.000870	0.000010	0.282183	0.000029	0.282181	-20.8	-17.3	1501	1888	-0.97
2.36	168	0.038203	0.000199	0.000876	0.000010	0.282187	0.000025	0.282184	-20.7	-17.1	1497	1881	-0.97
2.37	168	0.040087	0.000648	0.000892	0.000007	0.282267	0.000030	0.282264	-17.9	-14.3	1386	1737	-0.97
2.38	164	0.044868	0.000380	0.001146	0.000006	0.282197	0.000023	0.282193	-20.4	-16.9	1494	1866	-0.97
2.39	156	0.029631	0.000518	0.000817	0.000003	0.282237	0.000025	0.282235	-18.9	-15.6	1424	1794	-0.98
2.40	164	0.036974	0.000297	0.000774	0.000007	0.282186	0.000023	0.282184	-20.7	-17.2	1494	1883	-0.98
2.41	152	0.020345	0.000171	0.000474	0.000004	0.282213	0.000029	0.282212	-19.8	-16.5	1445	1836	-0.99
2.42	176	0.045478	0.000603	0.001614	0.000035	0.282347	0.000028	0.282342	-15.0	-11.4	1299	1595	-0.95
2.43	165	0.070178	0.000650	0.001456	0.000011	0.282240	0.000027	0.282236	-18.8	-15.3	1444	1789	-0.96
2.44	162	0.048778	0.000357	0.001221	0.000029	0.282204	0.000027	0.282200	-20.1	-16.7	1486	1854	-0.96
2.45	163	0.046546	0.000438	0.001056	0.000027	0.282223	0.000026	0.282219	-19.4	-16.0	1454	1819	-0.97
2.46	164	0.046155	0.000366	0.001228	0.000024	0.282216	0.000026	0.282212	-19.7	-16.2	1470	1832	-0.96
2.47	161	0.033566	0.000450	0.000732	0.000007	0.282147	0.000030	0.282145	-22.1	-18.7	1546	1954	-0.98
2.48	179	0.087910	0.002370	0.002042	0.000052	0.282328	0.000029	0.282321	-15.7	-12.0	1341	1631	-0.94
2.49	180	0.047267	0.000146	0.001133	0.000006	0.282365	0.000029	0.282361	-14.4	-10.6	1257	1559	-0.97
2.50	174	0.040239	0.000434	0.001252	0.000016	0.282107	0.000029	0.282103	-23.5	-19.9	1624	2024	-0.96
2.51	165	0.032778	0.000348	0.000797	0.000017	0.282274	0.000030	0.282272	-17.6	-14.1	1372	1725	-0.98
2.53	170	0.035147	0.000562	0.001092	0.000006	0.282200	0.000030	0.282196	-20.2	-16.6	1487	1859	-0.97
2.56	2488	0.011712	0.000164	0.000415	0.000003	0.281316	0.000024	0.281296	-51.5	3.7	2660	2713	-0.99
2.57	185	0.047108	0.000752	0.001264	0.000011	0.282446	0.000029	0.282441	-11.5	-7.6	1148	1413	

Table 4 (continued)

Spot	<i>t</i> (Ma)	$^{176}\text{Yb}/^{177}\text{Hf}$	$\pm 2\sigma$	$^{176}\text{Lu}/^{177}\text{Hf}$	$\pm 2\sigma$	$^{176}\text{Hf}/^{177}\text{Hf}$	$\pm 2\sigma$	$(^{176}\text{Hf}/^{177}\text{Hf})_{\text{i}}^{\text{a}}$	$\varepsilon_{\text{Hf}}(0)$	$\varepsilon_{\text{Hf}}(t)$	T_{DM1} (Ma)	T_{DM2} (Ma)	$f_{\text{Lu/Hf}}$
<i>12XTM01</i>													
3.8	164	0.022523	0.000435	0.000708	0.000012	0.282217	0.000016	0.282214	-19.6	-16.1	1449	1828	-0.98
3.9	168	0.031427	0.000804	0.000985	0.000026	0.282226	0.000015	0.282223	-19.3	-15.7	1446	1811	-0.97
3.10	131	0.033361	0.000087	0.001183	0.000001	0.282323	0.000019	0.282320	-15.9	-13.1	1317	1648	-0.96
3.11	2541	0.015889	0.000109	0.000593	0.000003	0.281345	0.000017	0.281316	-50.5	5.6	2633	2660	-0.98
3.12	2530	0.008661	0.000082	0.000347	0.000002	0.281226	0.000015	0.281209	-54.7	1.5	2776	2852	-0.99
3.13	182	0.039957	0.000881	0.001510	0.000027	0.282361	0.000017	0.282356	-14.5	-10.7	1275	1568	-0.95
3.14	2526	0.010413	0.000174	0.000392	0.000005	0.281239	0.000017	0.281220	-54.2	1.8	2761	2833	-0.99
3.15	128	0.029678	0.001103	0.001158	0.000040	0.282331	0.000022	0.282328	-15.6	-12.9	1306	1635	-0.97
3.16	175	0.086407	0.001252	0.002946	0.000053	0.282259	0.000021	0.282250	-18.1	-14.6	1476	1760	-0.91
4.1	162	0.043378	0.001117	0.001021	0.000028	0.282110	0.000030	0.282107	-23.4	-20.0	1609	2020	-0.97
4.2	163	0.015357	0.000571	0.000387	0.000015	0.282257	0.000026	0.282256	-18.2	-14.7	1381	1754	-0.99
4.3	2537	0.028540	0.001250	0.000695	0.000030	0.281318	0.000030	0.281284	-51.4	4.4	2677	2718	-0.98
4.4	2574	0.017826	0.000234	0.000487	0.000006	0.281286	0.000025	0.281262	-52.5	4.4	2705	2744	-0.99
4.6	2467	0.015047	0.000371	0.000388	0.000011	0.281232	0.000026	0.281214	-54.5	0.2	2771	2864	-0.99
4.7	2517	0.021623	0.001592	0.000522	0.000033	0.281253	0.000030	0.281228	-53.7	1.9	2752	2823	-0.98
4.9	123	0.062052	0.000150	0.001619	0.000007	0.282387	0.000030	0.282383	-13.6	-11.1	1242	1538	-0.95
4.12	167	0.054228	0.001902	0.001338	0.000039	0.282216	0.000026	0.282212	-19.7	-16.1	1474	1831	-0.96
4.13	2505	0.013838	0.000049	0.000389	0.000002	0.281308	0.000024	0.281289	-51.8	3.8	2669	2719	-0.99
4.14	157	0.035639	0.000383	0.000879	0.000009	0.282284	0.000029	0.282281	-17.3	-13.9	1362	1710	-0.97
4.15	2525	0.022322	0.000232	0.000555	0.000006	0.281298	0.000030	0.281271	-52.1	3.6	2694	2744	-0.98
4.17	2570	0.020069	0.000136	0.000521	0.000003	0.281295	0.000029	0.281270	-52.2	4.6	2695	2733	-0.98
4.18	2513	0.012160	0.000118	0.000423	0.000004	0.281281	0.000027	0.281261	-52.7	3.0	2707	2766	-0.99
4.20	2480	0.011577	0.000162	0.000348	0.000005	0.281311	0.000027	0.281295	-51.7	3.4	2662	2718	-0.99
4.21	160	0.039386	0.000160	0.000911	0.000005	0.282171	0.000026	0.282168	-21.3	-17.9	1520	1912	-0.97
4.23	168	0.041636	0.000411	0.000994	0.000008	0.282277	0.000030	0.282274	-17.5	-13.9	1375	1719	-0.97
4.24	126	0.092528	0.002818	0.002577	0.000066	0.282512	0.000030	0.282506	-9.2	-6.6	1092	1315	-0.92
4.26	2515	0.080907	0.002106	0.001841	0.000046	0.281388	0.000029	0.281299	-48.9	4.4	2661	2698	-0.94
4.27	162	0.094581	0.000712	0.002685	0.000053	0.282223	0.000030	0.282215	-19.4	-16.2	1519	1827	-0.92
4.31	2507	0.015290	0.000173	0.000392	0.000003	0.281271	0.000024	0.281252	-53.1	2.5	2719	2784	-0.99
4.32	159	0.063940	0.000470	0.001481	0.000025	0.282187	0.000025	0.282182	-20.7	-17.4	1521	1887	-0.96
4.33	176	0.018791	0.000346	0.000505	0.000005	0.282440	0.000023	0.282438	-11.7	-7.9	1133	1422	-0.98
4.34	158	0.032191	0.000260	0.000983	0.000015	0.282161	0.000026	0.282158	-21.6	-18.2	1536	1930	-0.97
4.39	125	0.073170	0.000670	0.002065	0.000011	0.282204	0.000030	0.282199	-20.1	-17.5	1521	1867	-0.94

Parameters used in the calculation are as follows: ^{176}Lu decay $\lambda = 1.867 \times 10^{-11} \text{ year}^{-1}$; $(^{176}\text{Lu}/^{177}\text{Hf})_{\text{CHUR}} = 0.0332$, $(^{176}\text{Hf}/^{177}\text{Hf})_{\text{CHUR}} = 0.282772$; $(^{176}\text{Lu}/^{177}\text{Hf})_{\text{DM}} = 0.0384$, $(^{176}\text{Hf}/^{177}\text{Hf})_{\text{DM}} = 0.28325$.

^a Calculated at single zircon U-Pb ages; $^{206}\text{Pb}/^{238}\text{U}$ ages for Mesozoic zircons; $^{207}\text{Pb}/^{206}\text{Pb}$ ages for Neoarchean to Early Paleoproterozoic zircons.

Table 5

In situ O isotopic compositions of zircons from the Xintai men rhyolite.

Spot	Raw $^{18}\text{O}/^{16}\text{O}$	$\pm 2\sigma$	$\delta^{18}\text{O}_{\text{SMOW}}$ (‰)	$\pm 2\sigma$ (‰)	Age	$\pm 1\sigma$
<i>Standard</i>						
FC-1 (n = 16)	0.0020328	0.0000010	5.61	0.16		
TEMORA-2 (n = 15)	0.0020376	0.0000011	8.05	0.15		
<i>12XTM01</i>						
12XTM01-1.1	0.0020339	0.0000003	6.20	0.14	164	6
12XTM01-2.1	0.0020353	0.0000003	6.90	0.17	2557	54
12XTM01-3.1	0.0020332	0.0000003	5.82	0.17	164	4
12XTM01-4.1	0.0020317	0.0000003	5.06	0.15	2488	5
12XTM01-5.1	0.0020340	0.0000004	6.21	0.17	167	4
12XTM01-8.1	0.0020328	0.0000003	5.65	0.16	160	3
12XTM01-11.1	0.0020327	0.0000003	5.60	0.16	2514	60
12XTM01-13.1	0.0020337	0.0000003	6.07	0.14	180	2
12XTM01-14.1	0.0020341	0.0000003	6.29	0.15	161	2
12XTM01-15.1	0.0020334	0.0000003	5.93	0.16	175	4
12XTM01-16.1	0.0020337	0.0000003	6.06	0.15	165	2
12XTM01-19.1	0.0020343	0.0000003	6.36	0.16	165	6
12XTM01-20.1	0.0020349	0.0000003	6.67	0.15	165	4
12XTM01-21.1	0.0020345	0.0000003	6.45	0.16	181	2
12XTM01-22.1	0.0020362	0.0000003	7.31	0.14	2528	6
12XTM01-23.1	0.0020331	0.0000003	5.79	0.14	2452	7
12XTM01-24.1	0.0020343	0.0000004	6.40	0.18	159	5
12XTM01-27.1	0.0020331	0.0000003	5.75	0.15	123	2
12XTM01-28.1	0.0020334	0.0000003	5.92	0.15	168	4
12XTM01-30.1	0.0020327	0.0000003	5.56	0.15	125	3
12XTM01-32.1	0.0020329	0.0000003	5.68	0.16	121	2

Correction for instrumental mass fractionation factor was done as following: $\delta^{18}\text{O}_{\text{VSMMW(Sample)}} = 5.61 + 1000 * [(\text{18O}/\text{16O})_{\text{Sample, measured}} - (\text{18O}/\text{16O})_{\text{FC-1, measured}}]/0.0020052$.

Ages are SHRIMP II zircon ages ($^{206}\text{Pb}/^{238}\text{U}$ ages for Mesozoic zircons and $^{207}\text{Pb}/^{206}\text{Pb}$ ages for Neoarchean to Early Paleoproterozoic zircons).

It is generally accepted that the Mesozoic geology of the eastern continental China continent was largely controlled by paleo-Pacific plate subduction (Niu, 2005; Niu et al., 2015; Wang et al., 2013; Wu et al., 2005a, 2011; S.-H. Zhang et al., 2014; Zhou et al., 2006;). However, the onset of paleo-Pacific plate subduction beneath eastern China remains controversial. Based on detrital zircon provenance data analyses, Li et al. (2006), X.-H. Li et al. (2012) and Z.-X. Li et al. (2012) proposed that an Early Permian active continental margin was developed in South China and thus paleo-Pacific plate subduction beneath South China began as early as in the Early Permian. It is also argued that paleo-Pacific plate subduction towards beneath NE China began in the Early Permian, based on the identification of island-arc gabbros of this age (Sun et al., 2015).

Alternatively, Kusky et al. (2014) suggested that the NCC shows no apparent effect from the paleo-Pacific plate subduction until the Early Jurassic. Before the Jurassic, the NCC had been isolated from South China and NE China and, as a result, should have experienced a different history of interactions between adjacent blocks. The pre-Jurassic tectonic evolution of the NCC was mainly controlled by collision between South and North China cratons in the south and the closure of Paleo-Asian Ocean in the north (e.g., Wang et al., 2015; S.-H. Zhang et al., 2014). After the closure of the Paleo-Asian and Paleo-Tethys oceans in the Late Paleozoic and Triassic, respectively, the NCC, South China and NE China amalgamated into a larger continent. In this model, the paleo-Pacific plate subduction began to affect the combined eastern continental China only since the Early Jurassic (~190 Ma). This scenario explains the large volumes of Jurassic and Cretaceous igneous rocks in eastern China with a unified NE-SW trend (e.g., Niu et al., 2015). Thus, the onset of paleo-Pacific plate subduction beneath the combined eastern continental China is most likely to be in the Early Jurassic (~190 Ma).

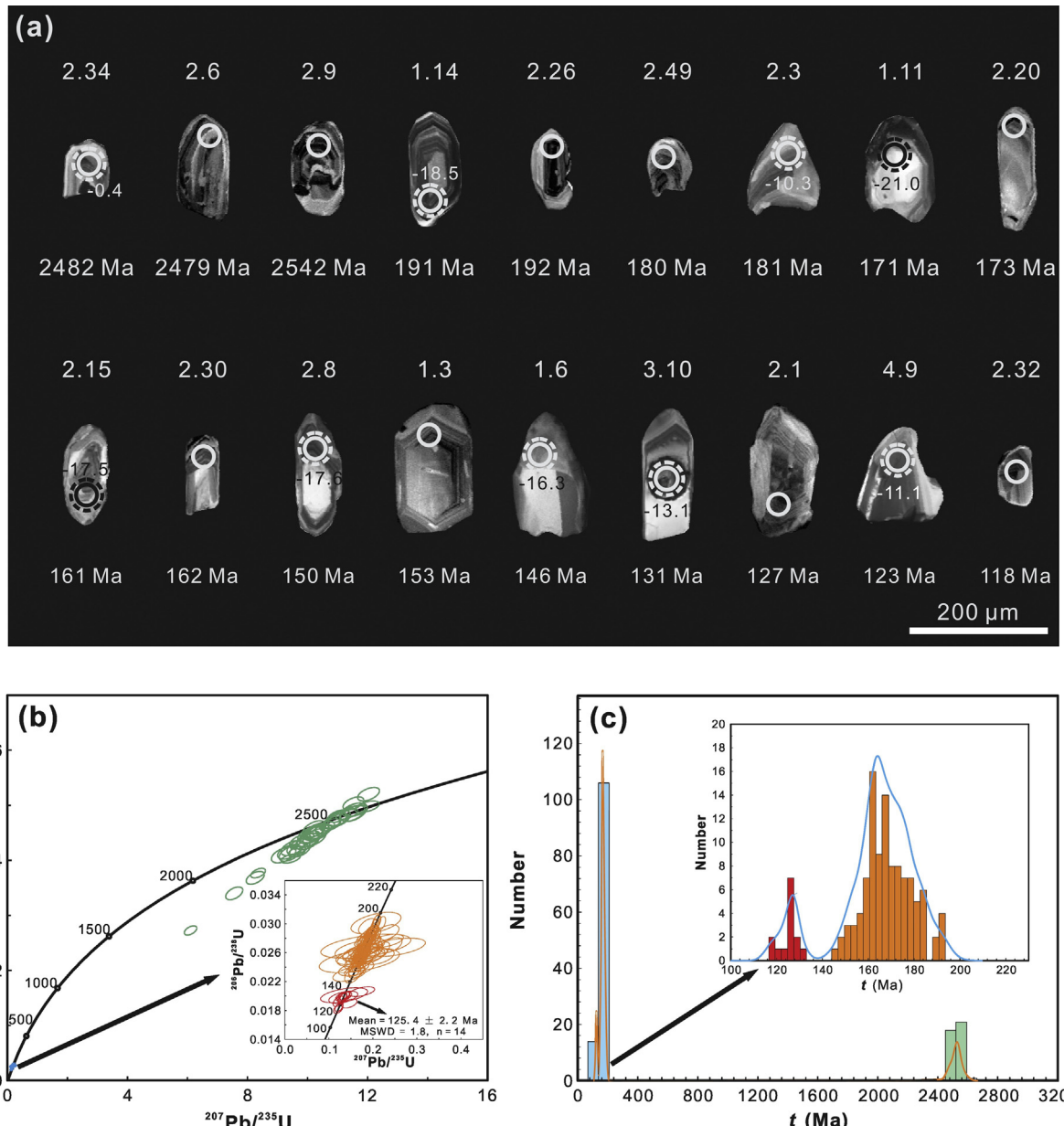


Fig. 3. (a) Cathodoluminescence (CL) images of representative zircons from the Xintaimen rhyolite. The solid and dashed circles on the CL images are the spots of *in situ* zircon U-Pb dating and Hf isotope analyses, respectively. Also shown are the single zircon ages ($^{206}\text{Pb}/^{238}\text{U}$ ages for Mesozoic zircons and $^{207}\text{Pb}/^{206}\text{Pb}$ ages for Neoarchean to Early Paleoproterozoic zircons) and $\varepsilon_{\text{Hf}}(t)$ values of zircons. (b) Zircon U-Pb concordia diagrams for the Xintaimen rhyolite. The mean is weighted average of $^{206}\text{Pb}/^{238}\text{U}$ ages at 95% confidence level. (c) Histograms of zircon U-Pb ages ($^{206}\text{Pb}/^{238}\text{U}$ ages for Mesozoic zircons and $^{207}\text{Pb}/^{206}\text{Pb}$ ages for Neoarchean to Early Paleoproterozoic zircons) for the Xintaimen rhyolite.

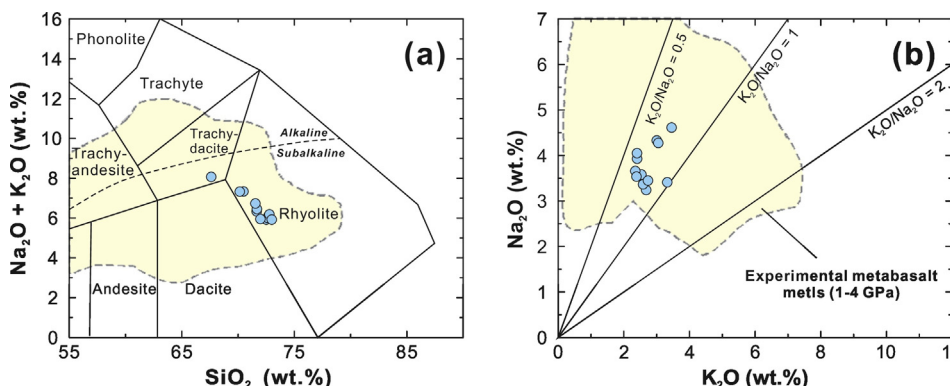


Fig. 4. (a) $(\text{Na}_2\text{O} + \text{K}_2\text{O})-\text{SiO}_2$ diagram and (b) $\text{Na}_2\text{O}-\text{K}_2\text{O}$ diagram for the Xintaimen rhyolite. The field of experimental metabasalt and eclogite melts at 1–4 GPa is constructed using the data from Rapp and Watson (1995), Rapp et al. (2003), Sen and Dunn (1994), Skjerlie and Patiño Douce (2002).

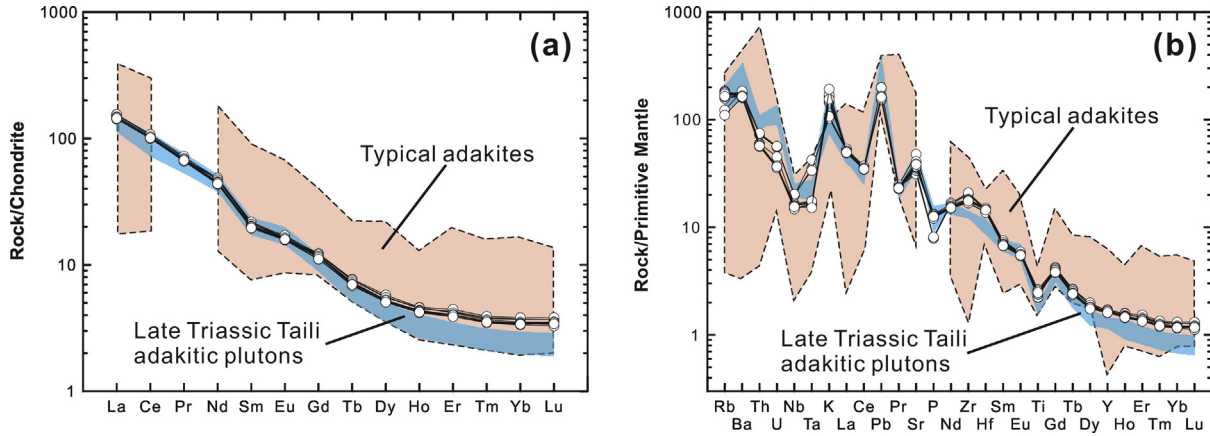


Fig. 5. (a) Chondrite-normalized REE patterns, and (b) primitive mantle (PM)-normalized trace element diagram for the Xintaimen rhyolite. The values of chondrite and PM are from Sun and McDonough (1989). Data sources: typical adakites, Defant et al. (1991) and Samaniego et al. (2005); Late Triassic Taili adakitic plutons, Wang et al. (2015).

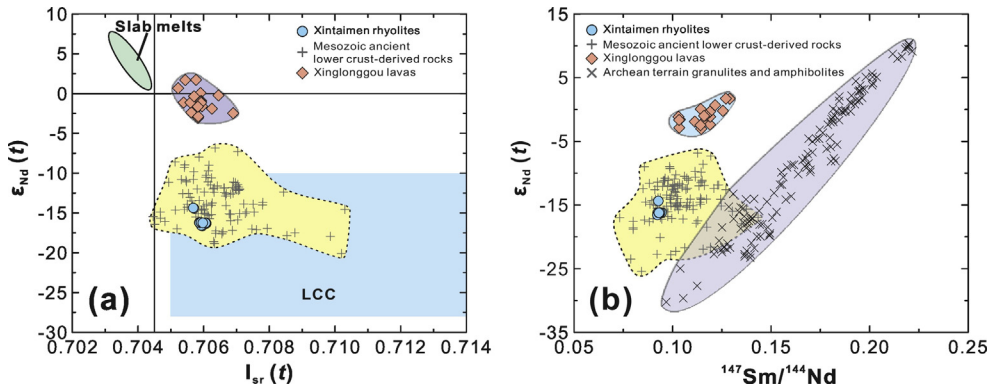


Fig. 6. (a) $\epsilon_{\text{Nd}}(t)$ - $I_{\text{sr}}(t)$ diagram and (b) $\epsilon_{\text{Nd}}(t)$ - $^{147}\text{Sm}/^{144}\text{Nd}$ diagram for the Xintaimen rhyolite. Also plotted for comparison are those of Xinglonggou lavas, Mesozoic lower crust-derived rocks, and terrain granulites and amphibolites in the NCC. Data sources: Xinglonggou lavas, Gao et al. (2004); Mesozoic ancient lower crust-derived rocks, Jiang et al. (2007), Ma et al. (2012), Wang et al. (2015), and references therein; Archean terrain granulites and amphibolites, Jiang et al. (2007), Wu et al. (2005c), and references therein.

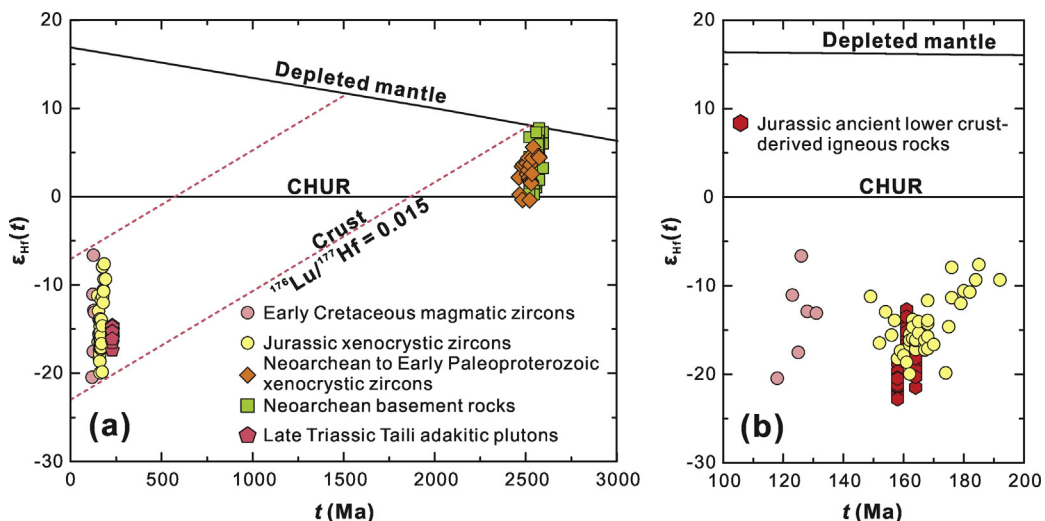


Fig. 7. (a) and (b) $\epsilon_{\text{Hf}}(t)$ - t diagram for zircons from the Xintaimen rhyolite. Note that (b) is enlarged part of the Mesozoic zircons in (a). Zircons from Neoarchean basement rocks, Late Triassic Taili adakitic plutons and Jurassic ancient lower crust-derived igneous rocks in western Liaoning are also plotted for comparison (Wang et al., 2015, 2016; X. Zhang et al., 2014).

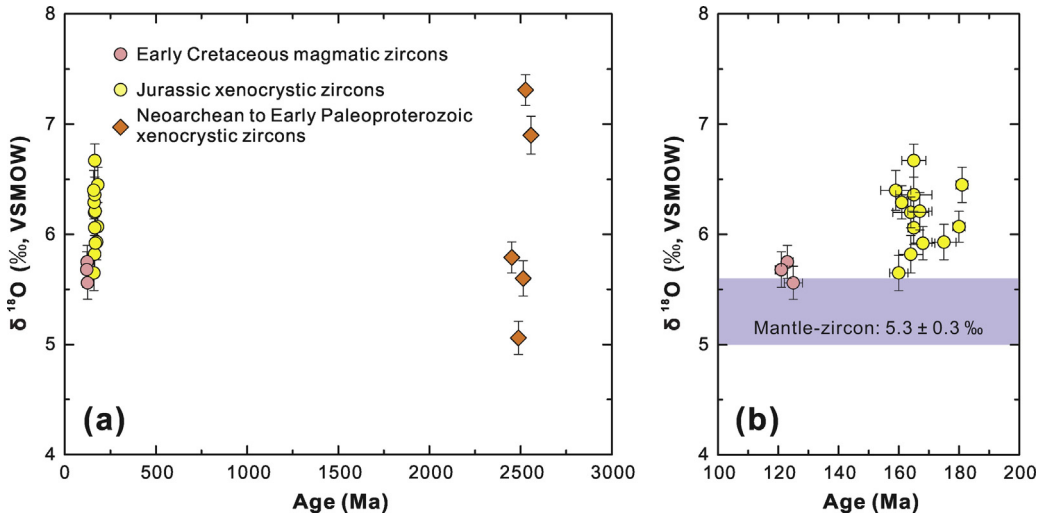


Fig. 8. (a) and (b) single zircon $\delta^{18}\text{O}$ -age diagrams for Mesozoic zircons from the Xintaimen rhyolite. (b) is enlarged part of the Mesozoic zircons in (a). Note that $^{206}\text{Pb}/^{238}\text{U}$ ages are used for Mesozoic zircons and $^{207}\text{Pb}/^{206}\text{Pb}$ ages for Neoarchean to Early Paleoproterozoic zircons in (b). Error bars are 2σ for $\delta^{18}\text{O}$ values and 1σ for single zircon ages, respectively. Mantle-zircon $\delta^{18}\text{O}$ values are from Valley (2003).

In summary, the Xintaimen adakitic rhyolite erupted in the Early Cretaceous, and formed through melting of Paleoproterozoic mafic lower crust. Isotopic similarities in primary and inherited zircons demonstrate that this melting process must have started at the onset of the paleo-Pacific plate subduction (~193 Ma), and continued for ~70 Myrs, until the late stage (~120 Ma) of paleo-Pacific plate subduction beneath the eastern continental China. Therefore, the Xintaimen adakitic rhyolite independently records a long-lived destruction/melting process

of the ancient lower crust of eastern China genetically related to the Paleo-Pacific plate subduction.

6. Conclusions

- (1) The Xintaimen adakitic rhyolite erupted during the Early Cretaceous (~125 Ma) with captured xenocrystic zircons of Neoarchean to Early Paleoproterozoic and Jurassic ages.

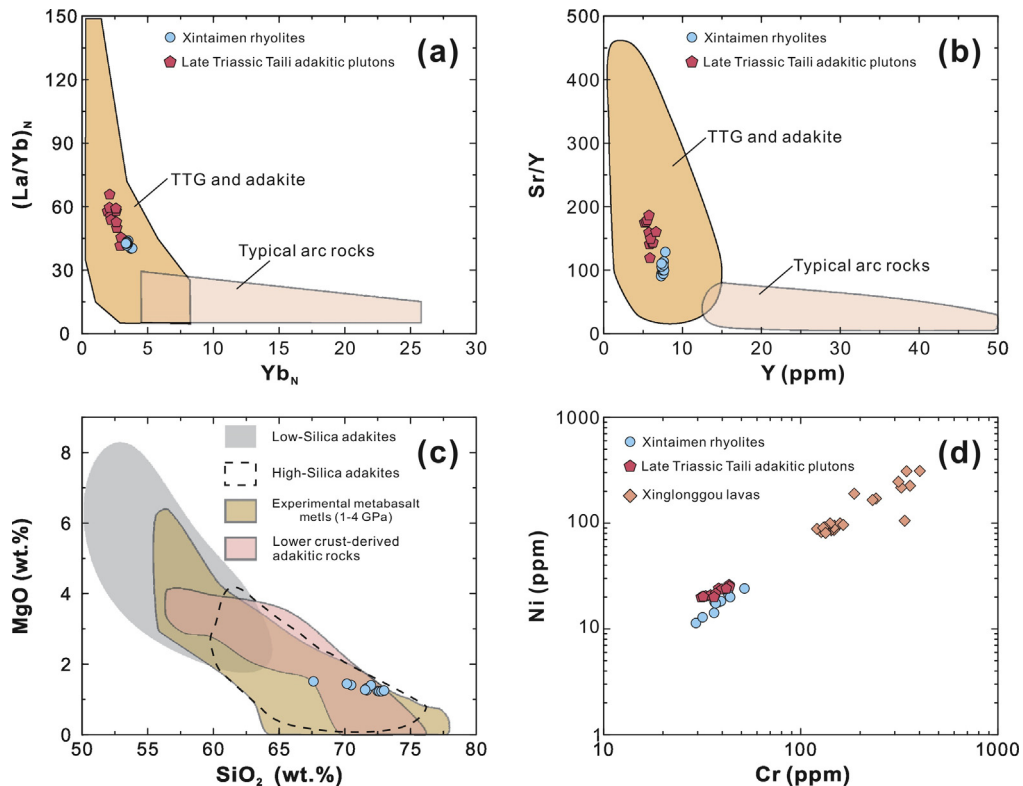


Fig. 9. Co-variation diagrams of (a) Chondrite-normalized $(\text{La}/\text{Yb})_N$ - $(\text{Yb})_N$, (b) Sr/Y - Y , (c) MgO - SiO_2 and (d) Ni - Cr for the Xintaimen rhyolite. Data sources of experimental metabasalt melts at 1–4 GPa are the same as in Fig. 4. The fields of low- and high-silica adakites are from Martin et al. (2005) and the field of lower crust-derived adakitic rocks is from Atherton and Petford (1993).

- (2) The magmas parental to the Xintaimen adakitic rhyolite were derived from partial melting of the Paleoproterozoic mafic lower crust, heated by mantle-derived mafic melts genetically associated with the paleo-Pacific plate subduction.
- (3) The Xintaimen adakitic rhyolite independently records a long-lived (~70 Myrs) melting process of ancient mafic lower crust, which is consistent with the time period of the paleo-Pacific plate subduction from the onset (~193 Ma) to the late stage (~120 Ma), and the destruction/melting process of the eastern continental China.

Acknowledgements

The authors are grateful to Dr. Hugh Smithies and an anonymous reviewer for their detailed and constructive peer-review comments, which greatly improved the quality of this paper. Editorial handling and critical comments by Editor-in-chief, Prof. Xian-Hua Li are also gratefully acknowledged. We also thank Wengang Liu and Wenping Zhu for helping with Sr-Nd isotope analysis. This study was supported by the National Natural Science Foundation of China (grant number 41430207, 41372060, 41572040, 41622202) and the National Key Basic Research Program of China (grant number 2013CB429806). Chao Wang wishes to acknowledge Chinese Scholarship Council for the financial support during his visit in Durham University (grant number 201606010063).

Appendix A. Supplementary data

Supplementary data to this article can be found online at <https://doi.org/10.1016/j.lithos.2017.09.031>.

References

- Atherton, M.P., Petford, N., 1993. Generation of sodium-rich magmas from newly underplated basaltic crust. *Nature* 362, 144–146.
- Chen, B., Jahn, B.M., Arakawa, Y., Zhai, M.G., 2004. Petrogenesis of the Mesozoic intrusive complexes from the southern Taihang Orogen, North China Craton: elemental and Sr-Nd-Pb isotopic constraints. *Contributions to Mineralogy and Petrology* 148, 489–501.
- Chen, B., Chen, Z.C., Jahn, B.M., 2009. Origin of mafic enclaves from the Taihang Mesozoic orogen, north China craton. *Lithos* 110, 343–358.
- Defant, M.J., Drummond, M.S., 1990. Derivation of some modern arc magmas by melting of young subducted lithosphere. *Nature* 347, 662–665.
- Defant, M., Clark, L., Stewart, R., Drummond, M., Boer, J., Maury, R., Bellon, H., Jackson, T., Restrepo, J., 1991. Andesite and dacite genesis via contrasting processes: the geology and geochemistry of El Valle Volcano, Panama. *Contributions to Mineralogy and Petrology* 106, 309–324.
- Eiler, J.M., 2001. Oxygen isotope variations of basaltic lavas and upper mantle rocks. *Reviews in Mineralogy and Geochemistry* 43, 319–364.
- Fu, B., Bröcker, M., Ireland, T., Holden, P., Kinsley, L.P.J., 2015. Zircon U-Pb, O, and Hf isotopic constraints on Mesozoic magmatism in the Cyclades, Aegean Sea, Greece. *International Journal of Earth Sciences* 104, 75–87.
- Gao, S., Rudnick, R.L., Yuan, H.L., Liu, X.M., Liu, Y.S., Xu, W.L., Ling, W.L., Ayers, J., Wang, X.C., Wang, Q.H., 2004. Recycling lower continental crust in the North China craton. *Nature* 432, 892–897.
- Gao, S., Rudnick, R.L., Xu, W.L., Yuan, H.L., Liu, Y.S., Walker, R.J., Puchtel, I.S., Liu, X.M., Huang, H., Wang, X.R., Yang, J., 2008. Recycling deep cratonic lithosphere and generation of intraplate magmatism in the North China Craton. *Earth and Planetary Science Letters* 270, 41–53.
- Guo, F., Li, H., Fan, W., Li, J., Zhao, L., Huang, M., Xu, W., 2015. Early Jurassic subduction of the Paleo-Pacific Ocean in NE China: petrologic and geochemical evidence from the Tumen mafic intrusive complex. *Lithos* 224–225, 46–60.
- Huppert, H.E., Sparks, R.S.J., 1988. The generation of granitic magmas by intrusion of basalt into continental crust. *Journal of Petrology* 29, 599–624.
- Ickert, R.B., Hiess, J., Williams, I.S., Holden, P., Ireland, T.R., Lanc, P., Schram, N., Foster, J.J., Clement, S.W., 2008. Determining high precision, in situ, oxygen isotope ratios with a SHRIMP II: analyses of MPI-DING silicate-glass reference materials and zircon from contrasting granites. *Chemical Geology* 257, 114–128.
- Ireland, T.R., Williams, I.S., 2003. Considerations in zircon geochronology by SIMS. *Reviews in Mineralogy and Geochemistry* 53, 215–241.
- Jiang, N., Liu, Y.S., Zhou, W.G., Yang, J.H., Zhang, S.Q., 2007. Derivation of Mesozoic adakitic magmas from ancient lower crust in the North China craton. *Geochimica et Cosmochimica Acta* 71, 2591–2608.
- Kusky, T.M., Windley, B.F., Wang, L., Wang, Z., Li, X., Zhu, P., 2014. Flat slab subduction, trench suction, and craton destruction: comparison of the North China, Wyoming, and Brazilian cratons. *Tectonophysics* 630, 208–221.
- Li, Z.-X., Li, X.-H., 2007. Formation of the 1300-km-wide intracontinental orogen and postorogenic magmatic province in Mesozoic South China: a flat-slab subduction model. *Geology* 35, 179–182.
- Li, X.-H., Li, Z.-X., Li, W.-X., Wang, Y., 2006. Initiation of the Indosinian Orogeny in South China: evidence for a Permian magmatic arc on Hainan Island. *The Journal of Geology* 114, 341–353.
- Li, X.-H., Li, Z.-X., He, B., Li, W.-X., Li, Q.-L., Gao, Y., Wang, X.-C., 2012a. The Early Permian active continental margin and crustal growth of the Cathaysia Block: in situ U-Pb, Lu-Hf and O isotope analyses of detrital zircons. *Chemical Geology* 328, 195–207.
- Li, Z.-X., Li, X.-H., Chung, S.-L., Lo, C.-H., Xu, X., Li, W.-X., 2012b. Magmatic switch-on and switch-off along the South China continental margin since the Permian: transition from an Andean-type to a Western Pacific-type plate boundary. *Tectonophysics* 532–535, 271–290.
- Liu, D.Y., Nutman, A.P., Compston, W., Wu, J.S., Shen, Q.H., 1992. Remnants of ≥3800 Ma crust in the Chinese part of the Sino-Korean craton. *Geology* 20, 339–342.
- Liu, J., Davis, G.A., Ji, M., Guan, H., Bai, X., 2008. Crustal detachment and destruction of the keel of North China craton: constraints from late mesozoic extensional structures. *Earth Science Frontiers* 15, 72–81.
- Liu, K., Zhang, J., Wilde, S.A., Zhou, J., Wang, M., Ge, M., Wang, J., Ling, Y., 2017. Initial subduction of the Paleo-Pacific Oceanic plate in NE China: constraints from whole-rock geochemistry and zircon U-Pb and Lu-Hf isotopes of the Khanka Lake granitoids. *Lithos* 274–275, 254–270.
- Ma, Q., Zheng, J.P., Griffin, W.L., Zhang, M., Tang, H.Y., Su, Y.P., Ping, X.Q., 2012. Triassic “adakitic” rocks in an extensional setting (North China): melts from the cratonic lower crust. *Lithos* 149, 159–173.
- Ma, Q., Xu, Y.-G., Zheng, J.-P., Griffin, W.L., Hong, L.-B., Ma, L., 2016. Coexisting early cretaceous high-Mg andesites and adakitic rocks in the North China craton: the role of water in intraplate magmatism and cratonic destruction. *Journal of Petrology* 57, 1279–1308.
- Martin, H., Smithies, R.H., Rapp, R., Moyen, J.F., Champion, D., 2005. An overview of adakite, tonalite-trondhjemite-granodiorite (TTG), and sanukitoid: relationships and some implications for crustal evolution. *Lithos* 79, 1–24.
- Menzies, M., Xu, Y.G., ZHANG, H.F., Fan, W.M., 2007. Integration of geology, geophysics and geochemistry: a key to understanding the North China Craton. *Lithos* 96, 1–21.
- Moyen, J.F., 2009. High Sr/Y and La/Yb ratios: the meaning of the “adakitic signature”. *Lithos* 112, 556–574.
- Niu, Y., 2005. Generation and evolution of basaltic magmas: some basic concepts and a new view on the origin of Mesozoic-Cenozoic basaltic volcanism in eastern China. *Geological Journal of China Universities* 11, 9–46.
- Niu, Y., 2014. Geological understanding of plate tectonics: basic concepts, illustrations, examples and new perspectives. *Global Tectonics and Metallogeny* 10, 23–46.
- Niu, Y., Tang, J., 2016. Origin of the Yellow Sea: an insight. *Science Bulletin* 61, 1076–1080.
- Niu, Y., Liu, Y., Xue, Q., Shao, F., Chen, S., Duan, M., Guo, P., Gong, H., Hu, Y., Hu, Z., Kong, J., Li, J., Liu, J., Sun, P., Sun, W., Ye, L., Xiao, Y., Zhang, Y., 2015. Exotic origin of the Chinese continental shelf: new insights into the tectonic evolution of the western Pacific and eastern China since the Mesozoic. *Science Bulletin* 60, 1598–1616.
- Peng, P., Guo, J., Zhai, M., Windley, B.F., Li, T., Liu, F., 2012. Genesis of the Hengling magmatic belt in the North China Craton: implications for Paleoproterozoic tectonics. *Lithos* 148, 27–44.
- Rapp, R.P., Watson, E.B., 1995. Dehydration melting of metabasalt at 8–32 kbar: implications for continental growth and crust-mantle recycling. *Journal of Petrology* 36, 891–931.
- Rapp, R.P., Shimizu, N., Norman, M.D., 2003. Growth of early continental crust by partial melting of eclogite. *Nature* 425, 605–609.
- Samaniego, P., Martin, H., Monzíer, M., Robin, C., Fornari, M., Eissen, J.-P., Cotten, J., 2005. Temporal evolution of magmatism in the Northern Volcanic Zone of the Andes: the geology and petrology of Cayambe Volcanic Complex (Ecuador). *Journal of Petrology* 46, 2225–2252.
- Sen, C., Dunn, T., 1994. Dehydration melting of a basaltic composition amphibolite at 1.5 and 2.0 GPa: implications for the origin of adakites. *Contributions to Mineralogy and Petrology* 117, 394–409.
- Skjerlie, K.P., Patiño Douce, A.E., 2002. The fluid-absent partial melting of a zoisite-bearing quartz eclogite from 1.0 to 3.2 GPa; implications for melting in thickened continental crust and for subduction-zone processes. *Journal of Petrology* 43, 291–314.
- Song, B., Nutman, A.P., Liu, D.Y., Wu, J.S., 1996. 3800 to 2500 Ma crustal evolution in the Anshan area of Liaoning Province, northeastern China. *Precambrian Research* 78, 79–94.
- Song, S.G., Niu, Y.L., Wei, C.J., Ji, J.Q., Su, L., 2010a. Metamorphism, anatexis, zircon ages and tectonic evolution of the Gongshan block in the northern Indo-China continent—an eastern extension of the Lhasa Block. *Lithos* 120, 327–346.
- Song, S.G., Su, L., Li, X.H., Zhang, G.B., Niu, Y.L., Zhang, L.F., 2010b. Tracing the 850-Ma continental flood basalts from a piece of subducted continental crust in the North Qaidam UHPM belt, NW China. *Precambrian Research* 183, 805–816.
- Sun, S.S., McDonough, W.F., 1989. Chemical and isotopic systematics of oceanic basalts: implications for mantle composition and processes. *Geological Society, London, Special Publications* 42, 313–345.
- Sun, M.-D., Xu, Y.-G., Wilde, S.A., Chen, H.-L., Yang, S.-F., 2015. The Permian Dongfanghong island-arc gabbro of the Wandashan Orogen, NE China: implications for Paleo-Pacific subduction. *Tectonophysics* 659, 122–136.
- Swisher, C.C., Wang, X., Zhou, Z., Wang, Y., Jin, F., Zhang, J., Xu, X., Zhang, F., Wang, Y., 2002. Further support for a Cretaceous age for the feathered-dinosaur beds of Liaoning, China: new $^{40}\text{Ar} \div ^{39}\text{Ar}$ dating of the Yixian and Tuchengzi formations. *Chinese Science Bulletin* 47, 136–139.
- Tang, J., Xu, W., Niu, Y., Wang, F., Ge, W., Sorokin, A.A., Chekryzhov, I.Y., 2016. Geochronology and geochemistry of Late Cretaceous–Paleocene granitoids in the Sikhote-Alin Orogenic Belt: petrogenesis and implications for the oblique subduction of the paleo-Pacific plate. *Lithos* 266–267, 202–212.
- Valley, J.W., 2003. Oxygen Isotopes in Zircon. *Reviews in Mineralogy and Geochemistry* 53, 343–385.

- Wang, Y., Fan, W., Zhang, G., Zhang, Y., 2013. Phanerozoic tectonics of the South China Block: key observations and controversies. *Gondwana Research* 23, 1273–1305.
- Wang, C., Song, S., Niu, Y., Su, L., 2015. Late Triassic adakitic plutons within the Archean terrane of the North China Craton: melting of the ancient lower crust at the onset of the lithospheric destruction. *Lithos* 212–215, 353–367.
- Wang, C., Song, S., Niu, Y., Wei, C., Su, L., 2016. TTG and potassiac granitoids in the Eastern North China craton: making Neoproterozoic upper continental crust during micro-continental collision and post-collisional extension. *Journal of Petrology* 57, 1775–1810.
- Wu, F.Y., Lin, J.Q., Wilde, S.A., Zhang, X.O., Yang, J.H., 2005a. Nature and significance of the Early Cretaceous giant igneous event in eastern China. *Earth and Planetary Science Letters* 233, 103–119.
- Wu, F.Y., Yang, J.H., Wilde, S.A., Zhang, X.O., 2005b. Geochronology, petrogenesis and tectonic implications of Jurassic granites in the Liaodong Peninsula, NE China. *Chemical Geology* 221, 127–156.
- Wu, F.Y., Zhao, G.C., Wilde, S.A., Sun, D.Y., 2005c. Nd isotopic constraints on crustal formation in the North China Craton. *Journal of Asian Earth Sciences* 24, 523–545.
- Wu, F., Yang, J., Zhang, Y., Liu, X., 2006. Emplacement ages of the Mesozoic granites in southeastern part of the Western Liaoning Province. *Acta Petrologica Sinica* 22, 315–325.
- Wu, F.-Y., Sun, D.-Y., Ge, W.-C., Zhang, Y.-B., Grant, M.L., Wilde, S.A., Jahn, B.-M., 2011. Geochronology of the Phanerozoic granitoids in northeastern China. *Journal of Asian Earth Sciences* 41, 1–30.
- Xiao, L., Clemens, J.D., 2007. Origin of potassiac (C-type) adakite magmas: experimental and field constraints. *Lithos* 95, 399–414.
- Xu, Y.G., 2001. Thermo-tectonic destruction of the archean lithospheric keel beneath the sino-korean craton in china: evidence, timing and mechanism. *Physics and Chemistry of the Earth, Part A: Solid Earth and Geodesy* 26, 747–757.
- Xu, W.L., Gao, S., Wang, Q.H., Wang, D.Y., Liu, Y.S., 2006. Mesozoic crustal thickening of the eastern North China craton: evidence from eclogite xenoliths and petrologic implications. *Geology* 34, 721–724.
- Xu, Y., Li, H., Pang, C., He, B., 2009. On the timing and duration of the destruction of the North China Craton. *Chinese Science Bulletin* 54, 3379–3396.
- Yang, W., Li, S., 2008. Geochronology and geochemistry of the Mesozoic volcanic rocks in Western Liaoning: implications for lithospheric thinning of the North China Craton. *Lithos* 102, 88–117.
- Yang, J.H., Wu, F.Y., 2009. Triassic magmatism and its relation to decratonization in the eastern North China Craton. *Science in China Series D: Earth Sciences* 52, 1319–1330.
- Yang, W., Li, S., Jiang, B., 2007. New evidence for Cretaceous age of the feathered dinosaurs of Liaoning: zircon U-Pb SHRIMP dating of the Yixian Formation in Sihetun, northeast China. *Cretaceous Research* 28, 177–182.
- Yang, J.H., Wu, F.Y., Wilde, S.A., Belousova, E., Griffin, W.L., 2008. Mesozoic decratonization of the North China block. *Geology* 36, 467–470.
- Yang, J.H., O'Reilly, S., Walker, R.J., Griffin, W., Wu, F.Y., Zhang, M., Pearson, N., 2010. Diachronous decratonization of the Sino-Korean craton: geochemistry of mantle xenoliths from North Korea. *Geology* 38, 799–802.
- Zhang, K.-J., 2012. Destruction of the North China Craton: lithosphere folding-induced removal of lithospheric mantle? *Journal of Geodynamics* 53, 8–17.
- Zhang, X., Zhang, H., Jiang, N., Wilde, S.A., 2010. Contrasting Middle Jurassic and Early Cretaceous mafic intrusive rocks from western Liaoning, North China craton: petrogenesis and tectonic implications. *Geological Magazine* 147, 844–859.
- Zhang, S.-H., Zhao, Y., Davis, G.A., Ye, H., Wu, F., 2014a. Temporal and spatial variations of Mesozoic magmatism and deformation in the North China Craton: implications for lithospheric thinning and decratonization. *Earth-Science Reviews* 131, 49–87.
- Zhang, X., Yuan, L., Wilde, S.A., 2014b. Crust/mantle interaction during the construction of an extensional magmatic dome: Middle to Late Jurassic plutonic complex from western Liaoning, North China Craton. *Lithos* 205, 185–207.
- Zhang, S.-H., Zhao, Y., Li, X.-H., Ernst, R.E., Yang, Z.-Y., 2017. The 1.33–1.30 Ga Yanliao large igneous province in the North China Craton: implications for reconstruction of the Nuna (Columbia) supercontinent, and specifically with the North Australian Craton. *Earth and Planetary Science Letters* 465, 112–125.
- Zhao, G.C., Sun, M., Wilde, S.A., Li, S.Z., 2005. Late Archean to Paleoproterozoic evolution of the North China Craton: key issues revisited. *Precambrian Research* 136, 177–202.
- Zheng, J., Griffin, W.L., O'Reilly, S.Y., Yang, J., Li, T., Zhang, M., Zhang, R.Y., Liou, J.G., 2006. Mineral chemistry of peridotites from Paleozoic, Mesozoic and Cenozoic lithosphere: constraints on mantle evolution beneath eastern China. *Journal of Petrology* 47, 2233–2256.
- Zhou, X., Sun, T., Shen, W., Shu, L., Niu, Y., 2006. Petrogenesis of Mesozoic granitoids and volcanic rocks in South China: a response to tectonic evolution. *Episodes* 29, 26.
- Zhou, J.-B., Cao, J.-L., Wilde, S.A., Zhao, G.-C., Zhang, J.-J., Wang, B., 2014. Paleo-Pacific subduction-accretion: evidence from Geochemical and U-Pb zircon dating of the Nadanhada accretionary complex, NE China. *Tectonics* 33 (2014TC003637).